# Monte Carlo and mean-field studies of successive phase transitions in rod monolayers

Diego Kramer and Avinoam Ben-Shaul
*Department of Physical Chemistry and The Fritz Haber Research Center for Molecular Dynamics, The Hebrew University, Jerusalem 91904, Israel*

Zhong-Ying Chen[a] and William M. Gelbart
*Department of Chemistry and Biochemistry, University of California, Los Angeles, California 90024*

(Received 31 July 1991; accepted 23 October 1991)

In this paper we present a rigid-rod model (involving a restricted set of orientations) which is solved first with mean-field theory and then by Monte Carlo simulation. It is shown that both interparticle attractions and anisotropic adsorption energies are necessary in order for two successive fluid–fluid transitions to occur. The first is basically a gas–liquid condensation of "lying down" rods in the plane of the surface, and the second involves a "standing up" of the particles. A close qualitative correspondence is established between the results obtained in the mean-field and Monte Carlo descriptions. The role of biaxial states, i.e., in-plane orientational ordering, is also discussed in both contexts. To this end, we develop an analogy between our one-component rod monolayer and a bidisperse system of interconverting isotropic particles.

## I. INTRODUCTION

Monolayers of amphiphilic molecules at air–water interfaces (also known as Langmuir monolayers[1,2]) are neither exactly two-dimensional (2D) nor three-dimensional (3D) systems. Because of the "head–tail" asymmetry of the amphiphiles, the symmetry of monolayers is lower than that of purely 2D or 3D systems—a fact reflected in their phase behavior.[2,3-7] Another important aspect of the monolayer phase behavior is the ability of the constituent molecules to respond to changes in density and/or temperature by altering their shape and orientation.

The monolayer's free energy $F$ may be represented as a sum of three terms $F = F_{\text{conf}} + F_{\text{trans}} + F_{\text{att}}$.[8] The conformational free energy $F_{\text{conf}} = Nf_{\text{conf}}$ is a sum of single molecule terms incorporating contributions from internal degrees of freedom (e.g., internal rotations around tail bonds), overall rotations of the tail chain, and molecule–surface interactions. $F_{\text{trans}}$ represents the two-dimensional translational entropy of the molecules, including the effects of excluded-area interactions, e.g., in the van der Waals(vdW) approximation $F_{\text{trans}} \simeq -NkT\ln(A - bN)$ with $A$ denoting the interfacial area and $b$ the excluded area per molecule. The third term accounts for *inter* molecular attractions.

At low densities, when interaction effects are negligible, the amphiphiles are in a state of maximal conformational freedom so that $f_{\text{conf}}$ is minimal. The tails of these "free" molecules are usually characterized by a globular, or "expanded," shape.[8] At low densities ($\rho = N/A$) the globules form a 2D gas. If intermolecular attractions are strong enough (i.e., $T$ is below the critical temperature) then, as $\rho$ increases the globules will eventually condense to a liquid. The gas–liquid transition is governed primarily by a trade-off between $F_{\text{trans}}$ and $F_{\text{att}}$, i.e., a loss in translational entropy of the gas phase for a gain in attractive potential energy in the liquid phase. The internal degrees of freedom are reluctant to participate in this transition since $F_{\text{conf}}$ is already minimal, particularly so if small changes in shape or orientation involve a high free energy price $\Delta F_{\text{conf}}$. In this case the gas–liquid transition is, to a good approximation, a simple condensation of free chain globules. Thus the area per molecule $a = A/N = 1/\rho$ in the liquid phase is similar to the cross sectional area, $a_f$, of the adsorbed free molecule ("free" in the sense of not being interfered with by other molecules—it is still constrained, however, by virtue of being excluded from the water substrate). The "order parameter" of this transition is the 2D density of unperturbed molecules.

As the monolayer is compressed further the molecules must stretch out (if they are flexible) and/or desorb some of their segments from the surface and stand upright, so as to occupy less surface area. This transition may be discontinuous (i.e., first-order) if, following the conformational change, the molecules can get considerably closer to each other, thus increasing the number of interchain (segment–segment) contacts. In other words, this transition is governed primarily by an interplay between $F_{\text{conf}}$ and $F_{\text{att}}$. The change in $a$ at the transition is, roughly, from $a_f$ to $a_m$, with $a_m$ denoting the cross sectional area of a fully stretched (upright) molecule. The degree of chain stretching/alignment or the monomer (segment) density may be taken to represent the order parameter of the transition.

The qualitative scheme outlined above was proposed earlier[8] as a possible explanation of the two successive fluid–fluid transitions which have been observed in various surfactant monolayers. The analogy was drawn between (i) the gas–liquid-expanded (*g–le*) transition in monolayers[3(a),4] and the condensation of free chains, and (ii) between the liquid-expanded–liquid-condensed (*le–lc*) transition and

[a] Present address: Eos Technologies, 1601 North Kent St. 1102 Arlington, Virginia 22209.

 0021-9606/92/032236-17$06.00 

the conformational/orientational transition described above. This qualitative picture is consistent with some other studies of the monolayer phase behavior.[9-11] In particular, Shin *et al.*[9] have carried out a mean-field analysis of a monolayer of flexible model chains. At low densities their (free) chains are strongly adsorbed to the surface, implying large cross sectional area per chain, $a_f$. They find two successive transitions: one (corresponding to the *g–le* transition) is characterized by "in-plane" condensation of the strongly adsorbed chains, while the second (*le–lc*) involves "out-of-plane" stretching and concomitant crowding of the chains.

If the qualitative notions outlined above regarding the origin of the monolayer's phase transitions are valid, then it might be possible to confirm and analyze them in simple model systems. The basic requirement from such models is to allow the adsorbed particles to change their cross-sectional area in response to lateral pressure. Then, in order to observe two successive monolayer transitions, this change must involve a high free energy price, which can only be compensated for at high densities—by favorable anisotropic intermolecular attractions between the particles in their upright (small area) orientation. If either of these condition is not fulfilled the two transitions will coalesce into a single transition.

The simplest conceivable monolayer models are those involving particles with two (or few) internal states.[11-14] One can consider for instance a "chemical" mixture of interconverting large and small disks[12] representing, respectively, the expanded and condensed states of the molecules. Large adsorption energy and/or degeneracy may be assigned to the large disks, to mimic their favorable $f_{\text{conf}}$. Various lattice-type models[14] of this kind have been proposed to account for the monolayer phase behavior. In such models each site is occupied by either a large or a small particle so that $\rho$ is constant. Only one type of phase transition, involving a change in the chemical composition of large vs small particles, is possible in these systems, resembling the *le–lc* transition. To account for the possibility of a condensation-type transition, the overall particle density should be a variable. In the lattice picture this amounts to adding vacancies as a third component. An extended spin-Hamiltonian approach of this type is described by Costas *et al.*[15] Recently, Zuckermann *et al.*[12] have presented a Monte Carlo study of a monolayer of interconverting hard disks. They focus on the phase behavior in the high density regime and find two transitions, one corresponding to a change in the composition (which may be compared to the *le–lc* transition) and the other to an ordering, liquid–solid, transition of small disks.

Another class of simple monolayer models is that of grafted mobile rods.[16-20] The rods may be regarded as the "stiff chain" limit of surfactant tails in a Langmuir monolayer, or as a realistic model of elongated rigid molecules adsorbed at one of their ends to a 2D surface. Moreover, a system of mobile grafted rods is of considerable interest in its own right. As is well known,[21-23] 3D and 2D systems of rodlike particles have long served as model systems for liquid–crystalline materials. As we shall see in the next sections, some of the more interesting aspects of grafted rods are related to several qualitative differences between their phase behavior as compared to that of rods in the bulk.

One of the first studies of rod monolayers is due to Boehm and Martire.[16] They applied DiMarzio's combinatoric algorithm[24] to calculate the configurational entropy of prolate parallelepipeds on a square lattice, and a Bragg–Williams approximation for the attractive free energy. The effects of excluded area interactions enter through the configurational entropy. These authors found only one first-order transition, in which both the density and the orientational distributions change simultaneously. In this study the rods were restricted to three possible orientations, two ($x$ and $y$) in which the rods lie on the surface and one upright ($z$). Similar models, in the spirit of Zwanzig's restricted orientation scheme[22] for the isotropic–nematic (I–N) transition of liquid crystals, were used by Chen *et al.*[18] and by Wang.[19]

Recently it has been shown[17,18] that a system of *hard* mobile grafted rods does not exhibit a first order I–N transition. This conclusion should be contrasted with the behavior of hard rods in 3D. There, as first shown by Onsager,[21] the gain in translational entropy (lower excluded volume) can compensate at sufficiently high densities for the loss in orientational entropy and induce a first order transition. Halperin *et al.*[17] have applied Onsager's approach to a monolayer of grafted hard spherocylinders and found (via simple functional forms for the orientational distribution function and numerical solution of the self-consistent equations) that the orientational order parameter increases monotonically and continuously with $\rho$. Based on a Landau-type analysis of a monolayer of rods with restricted orientations (Zwanzig's model),[22] Chen *et al.*[18] have shown that the absence of a first-order transition in a monolayer of hard rods is due to the broken symmetry of its excluded area matrix, as compared to the corresponding 3D case. They have also predicted that when attraction is added to the rod–rod potential the monolayer can exhibit a first-order orientational phase transition in which the rods stand up from the surface. This was confirmed by Monte Carlo (MC) computations for spherocylinders with continuous orientations. The simulations also indicate, in agreement with the Landau analysis for restricted orientations, the possibility of an orientational phase transition to a biaxial state, involving rod ordering in the surface plane. The coupling between the two types of orientational transitions (the standing-up and in-plane) and the gas liquid transition has been examined in some detail by Wang[19] on the basis of a generalized van der Waals approach.[25] One of his conclusions was that if the attractive interactions are anisotropic, and the adsorption energy is large, a first-order in-plane ordering transition can take place, leading to a discontinuous jump in the relative proportions of in-plane and upright rods.

The present paper also deals with the phase behavior of a system of mobile grafted rods, and all of the analysis is based on a monolayer version of the restricted orientation model.[22] We present both MC (lattice) simulations and mean-field theory for this system. Our primary goal is to examine the validity of the qualitative ideas mentioned above regarding the nature of the two successive fluid–fluid transitions, and the conditions responsible for their appearance. In particular, we analyze the effects of excluded area

interactions, isotropic and orientation dependent attractions, and adsorption energy. These are the molecular factors which govern the interplay between the various contributions to the monolayer's free energy. We use a generalized vdW-mean-field theory to establish several basic results concerning the differences between the monolayer and the 3D behavior, and then check these conclusions via direct MC simulation of the same system. The role of biaxiality in each of these contexts is also discussed. In particular, we treat in detail a system of interconverting isotropic particles of different sizes and develop an analogy between their phase behavior and that obtained for reorienting rodlike molecules.

## II. THE MODEL

We consider a system of $N$ rodlike particles which are adsorbed on a planar surface of area $A$. The rods are mobile, but one of their ends (the "head") is always in contact with the surface, which we take as the $xy$ plane. We use $\mathbf{r}_i = x_i, y_i$ to denote the position of the head of rod $i$ on the surface, and $\Omega_i = \theta_i, \phi_i$ for its orientation. As usual $\phi_i$ is the azimuthal angle and $\theta_i$ $(0 \leqslant \theta_i \leqslant \pi/2)$ is the angle between the rod and the $z$ axis which is normal to the surface. The configuration of the monolayer is fully specified by $\mathbf{r}^N$, $\Omega^N$ with the notation, $\mathbf{r}^N = \mathbf{r}_1,...,\mathbf{r}_N$; $\Omega^N = \Omega_1,...,\Omega_N$.

The potential energy of the monolayer is written quite generally as a sum of one-body and pair-interaction contributions, as follows:

$$U(\mathbf{r}^N,\Omega^N) = \sum_i \epsilon(\Omega_i) + \sum_{i<j} u_r(\mathbf{r}_{ij},\Omega_i,\Omega_j) + \sum_{i<j} u_a(\mathbf{r}_{ij},\Omega_i,\Omega_j). \quad (1)$$

Here $\epsilon(\Omega)$ denotes the orientation-dependent energy of adsorption, or rod–surface interaction. Note that $\epsilon(\Omega)$ can also be thought of as an effective free energy, since the modeling of semiflexible surfactants by rigid rods involves the implicit suppression of internal, i.e., conformational, degrees of freedom. More explicitly, in this case the adsorption energy stands for $\epsilon(\Omega) = -kT \ln q(\Omega)$, where $q(\Omega)$ is the orientation-dependent internal partition function for an adsorbed molecule. $u_r$ represents the short-ranged repulsive interaction between pairs of particles, modeled here by excluded-volume forces. More explicitly,

$$u_r(\mathbf{r}_{ij},\Omega_i,\Omega_j) = \begin{cases} \infty, & \text{overlapping hard cores} \\ 0, & \text{otherwise.} \end{cases} \quad (2)$$

Finally, $u_a$ denotes the attraction energy associated with a pair of particles whose heads (or centers of mass) are separated by $\mathbf{r}_{ij} = |\mathbf{r}_j - \mathbf{r}_i|$ and whose orientations are $\Omega_i$ and $\Omega_j$. To further specify $u_a(\mathbf{r}_{ij},\Omega_i,\Omega_j)$, and to be more precise about the energies $\epsilon(\Omega_i)$ and $u_r(\mathbf{r}_{ij},\Omega_i,\Omega_j)$, we introduce a particular choice for the shape of the rodlike particles. Also, since the generalized mean-field theory described below is most incisively analyzed for the case of discretized positions and orientations, we need to consider the above interaction model in the specific context of an appropriate lattice.

Let each rigid, rodlike, particle be described as a rectangular parallelepiped of length $l$ and square cross section $d \times d$. Let the axial ratio $l/d$ be denoted by $\chi$. For convenience we shall put $d = 1$, i.e., measure all lengths in units of of $d$, so that $\chi = l$. In our Monte Carlo simulation the planar surface on which rods are adsorbed (i.e., the $xy$ plane) is represented by a square lattice, each of whose sites of area $d^2 = 1$ can accommodate one rod in the upright ($z$) direction. A lying-down rod, on the other hand, occupies a row of $\chi$ nearest-neighbor sites along a direction parallel to the $x$ or $y$ axes. Thus only three orientations are allowed for the rods, $\Omega = x$ or $y$ (lying down) or $\Omega = z$ axis (standing up). The same model is employed in our mean-field analysis of the monolayer. In this case, however, the discretization of the $xy$ plane is not necessary and, in fact, not used explicitly.

For the above model it is clear that the one-body adsorption energy can take on one of two values, according to whether the rod is lying down or standing up:

$$\epsilon(\Omega) = \begin{cases} -\chi\epsilon kT, & \Omega = x \text{ or } y \\ -\epsilon kT, & \Omega = z. \end{cases} \quad (3)$$

That is, $\epsilon kT$ can be thought of as the adsorption energy per rod "segment" in contact with the surface. Similarly, treating the pair attractions between rods as a sum of nearest-neighbor segment–segment contributions we write

$$u_a(\mathbf{r}_{ij},\Omega_i,\Omega_j) = -nukT. \quad (4)$$

Here $n$ is the number of nearest-neighbor segment–segment contacts for the configuration $\mathbf{r}_{ij}$, $\Omega_i$, $\Omega_j$, and $ukT$ is the attraction energy associated with a single pair of nearest-neighbor segments. Thus, for example, any configuration of perpendicular rods corresponds to $u_a = -ukT$ if the particles are touching (and zero otherwise), whereas parallel rods along $x$ or $y$ have $u_a$'s ranging from $-ukT$ to $-\chi ukT$ as they move along each other in neighboring rows, etc. The only exception to Eq. (4) is the configuration of two $z$ rods on neighboring sites, for which we take $u_a = -\alpha\chi ukT$, with $\alpha$ serving as a measure of the anisotropy of the attractive interactions; $\alpha > 1$ corresponds to stronger attractions between segments of $z$ rods.

In the generalized van der Waals formulation used below to treat the above system in mean-field approximation, it is convenient to consider first the case of continous orientations and to specialize to discretized values ($x$, $y$, and $z$) only when we need to explicitly evaluate the pair excluded-areas and effective attraction energies which arise naturally there.

## III. MEAN-FIELD ANALYSIS

### A. Free energies and order parameters

Generalized van der Waals theory[25-27] provides a systematic way to treat the competing roles of interparticle repulsions and attractions in determining the phase behavior of fluids. In the original formulation of Kac, Uhlenbeck, and Hemmer[26] and Longuet-Higgins and Widom,[27] which dealt specifically with simple liquids, (i.e., no anisotropy or internal degrees of freedom), the rigid core effects were treated essentially exactly, with the long-ranged attractive forces entering via a mean-field averaging. More generally, for a sys-

tem such as ours where the (hard rod) particle anisotropy may give rise to long-range orientational order, we can write the system free energy as

$$F(\{N_\Omega\},A,T) = F_{\rm hr}(\{N_\Omega\},A,T) + N\sum_\Omega P_\Omega \Psi(\Omega), \tag{5}$$

where $\{N_\Omega\}$ describes the distribution of particle orientations and $\Psi(\Omega)$ is the effective attraction felt by a particle with orientation $\Omega$. $P_\Omega = N_\Omega/N$ is the fraction of rods in orientation $\Omega$.

For systems of symmetrical particles (e.g., attracting spheres in 3D or disks in 2D) Eq. (5) reduces to the ordinary vdW equation and its attendant predictions for the gas–liquid transition. For anisotropic (e.g., rodlike or disklike) particles in 3D it can be reduced[25] to Onsager's[21] or Maier–Saupe's[28] theories of the isotropic–nematic (I–N) transition in liquid crystals. It should be recalled that in Onsager's theory the I–N transition is driven by the anisotropy of the hard core (excluded volume) interactions, while the attractive part of the potential is totally irrelevant. In Maier–Saupe's theory, the role of $u_r$ and $u_a$ is reversed, i.e., the transition is dominated by the anisotropy of $u_a$. Alternatively, following power series expansion in the appropriate "order parameter," the generalized vdW free energy becomes a Landau–de Gennes-type free energy, enabling analysis of the phase behavior from yet another angle.[18] Thus the generalized vdW equation provides a versatile tool for incorporating the various contributions to the system's free energy and for elucidating their roles in different phase transitions. We shall therefore adopt it as a starting point for analyzing the phase behavior in a monolayer of grafted rods.

In the Appendix we show that some straightforward approximations allow Eq. (5) to be rewritten in the form

$$\beta F/N = \ln\rho - 1 + \sum_\Omega P_\Omega[\ln P_\Omega + \beta\epsilon(\Omega)] - \ln(1-\rho\langle b\rangle) - \beta\langle a\rangle\rho. \tag{6}$$

Here $\rho = N/A$ is the 2D number density, and

$$\langle b\rangle = \sum_{\Omega,\Omega'} P_\Omega P_{\Omega'} b_{\Omega\Omega'} = \left\langle -\frac{1}{2}\int d\mathbf{r} f_{\rm hr}(\mathbf{r},\Omega,\Omega')\right\rangle \tag{7}$$

is the average vdW "$b$" coefficient in "mixture of composition" $\{P_\Omega\}$. $f_{\rm hr}(\mathbf{r},\Omega,\Omega')$ is the hard-rod Mayer function whose integral over $\mathbf{r}$ gives the excluded area $b_{\Omega,\Omega'}$ for two rods in orientations $\Omega$ and $\Omega'$. Similarly,

$$\langle a\rangle = \sum_{\Omega,\Omega'} P_\Omega P_{\Omega'} a_{\Omega\Omega'} = \left\langle -\frac{1}{2}\int d\mathbf{r}[f_{\rm hr}(\mathbf{r},\Omega,\Omega')+1]u_a(\mathbf{r},\Omega,\Omega')\right\rangle \tag{8}$$

is a generalized vdW "$a$" coefficient. Note that the factor $f_{\rm hr}+1$ restricts the average over $u_a$ to nonoverlapping hard core configurations. Finally, the free energy in Eq. (6) can be rewritten exactly in the alternately suggestive form

$$\beta F/N = \ln(\rho/ez^0) + \sum_\Omega P_\Omega \ln(P_\Omega/P^0_\Omega) - \ln(1-\rho\langle b\rangle) - \beta\langle a\rangle\rho, \tag{9}$$

where we have incorporated the adsorption energy term $\Sigma P_\Omega \epsilon(\Omega)$ into the mixing entropy term $\Sigma P_\Omega \ln P_\Omega$ through the definitions

$$P^0_\Omega = \exp[-\beta\epsilon(\Omega)]/z^0, \tag{10}$$

$$z^0 = \sum_\Omega \exp[-\beta\epsilon(\Omega)]. \tag{11}$$

Here $P^0_\Omega$ is the orientational probability distribution function (pdf) in the limit $\rho\to 0$, and $z^0$ is the corresponding molecular partition function. It is easily confirmed that $P^0_\Omega$ is, indeed, the pdf which minimizes $F$ when $\rho\to 0$. Explicitly, from Eq. (9) we see that in this limit $\Sigma P_\Omega \ln(P_\Omega/P^0_\Omega)$ is the only $P_\Omega$ dependent term. Since $\ln x \geqslant 1 - 1/x$ for all $x>0$ we can write $\ln(P_\Omega/P^0_\Omega)\geqslant 1 - P^0_\Omega/P_\Omega$. Multiplying the inequality by $P_\Omega$ and summing over $\Omega$ we find $\Sigma P_\Omega \ln(P_\Omega/P^0_\Omega)\geqslant 0$. The equality, which corresponds to minimal $F$, holds only when $P_\Omega = P^0_\Omega$. Thus, as $\rho\to 0$, we get $F = NkT\ln(\rho/z^0 e)$, as expected.

Expanding the third (hard core) term in Eq. (9) yields

$$\beta F/N = \ln(\rho/ez^0) + \sum_\Omega P_\Omega \ln(P_\Omega/P^0_\Omega) + \tfrac{1}{2}\langle w\rangle\rho + C\rho^2 + O(\rho^3). \tag{12}$$

Here $C = \langle b\rangle^2$ and

$$\langle w\rangle = \sum_{\Omega,\Omega'} P_\Omega P_{\Omega'} w_{\Omega\Omega'} \tag{13}$$

with

$$w_{\Omega\Omega'} = 2(b_{\Omega\Omega'} - \beta a_{\Omega\Omega'}) \tag{14}$$

denoting the *effective* interaction free energy (in units of $kT$) between two rods in orientations $\Omega$ and $\Omega'$. In the third term of Eq. (12), $\langle w\rangle/2 = B$ is the second virial coefficient corresponding to the vdW equation. As is well known, $B$ is the high temperature approximation to the exact second virial coefficient $\tilde{B}$ [for a pair potential of the form (1)]. Larger differences exist between $C = \langle b\rangle^2$ and $\tilde{C}$, and between the $O(\rho^3)$ terms and higher virial coefficients.

From Eq. (9) we obtain the generalized vdW equation for the monolayer's 2D pressure, $\Pi = \rho^2[\partial(F/N)/\partial\rho]$:

$$\beta\Pi = \rho/(1-\langle b\rangle\rho) - \beta\langle a\rangle\rho^2. \tag{15}$$

Similarly, from the virial form (12) or the expansion of Eq. (15) we get $\beta\Pi = \rho + (\langle w\rangle/2)\rho^2 + C\rho^3 + \cdots$. An explicit expression for the chemical potential $\mu$ then follows from $\mu = F/N + \Pi/\rho$.

Let $\Delta P_\Omega = P_\Omega - P^0_\Omega$ denote the difference between the actual $P_\Omega$ and its value at $\rho = 0$. Also, let $F^0 = F(\{N^0_\Omega\},A,T)$ denote the free energy (at finite density) assuming that $P_\Omega = P^0_\Omega = N^0_\Omega/N$, independent of $\rho$. Indeed, $P_\Omega$ is constant over a wide range of densities for many systems, e.g., for the gas phase or isotropic-liquid phase of rodlike molecules in 3D. It does not hold for grafted rods, however, as we shall see below.

Corresponding to $\{\Delta P_\Omega\}$ one can define an orientational free energy $\hat{F}$ via

$$F = F^0 + \hat{F}, \tag{16}$$

so that $\hat{F} = 0$ for $P_\Omega = P^0_\Omega$ ($\Delta P_\Omega = 0$). If we use Eq. (12) for $F$, then

$$\beta F^0/N = \ln(\rho/ez^0) + \tfrac{1}{2}\langle w\rangle^0\rho + C^0\rho^2 + O(\rho^3), \tag{17}$$

where $\langle w\rangle^0$ is the zero density limit of $\langle w\rangle$, cf. Eq. (13). ($B^0 = \langle w\rangle^0/2$, $C^0$, etc., are the virial coefficients for a mixture of rods with fixed composition $P^0_\Omega$.) For $\hat{F}$ we get

$$\begin{aligned}\beta\hat{F}/N &= \sum_\Omega P_\Omega \ln(P_\Omega/P^0_\Omega) + \frac{1}{2}\rho[\langle w\rangle - \langle w\rangle^0] + O(\rho^2)\\ &= \sum_\Omega P_\Omega \ln(P_\Omega/P^0_\Omega)\\ &\quad + \frac{1}{2}\rho\sum_{\Omega,\Omega'}(P_\Omega P_{\Omega'} - P^0_\Omega P^0_{\Omega'})w_{\Omega\Omega'} + O(\rho^2).\end{aligned} \tag{18}$$

Since all the $P_\Omega$ dependence of $F$ appears in $\hat{F}$, the equilibrium $P_\Omega$ for every value of $\rho$ corresponds to a minimum of $\hat{F}$. One, or several, *orientational order parameters* can be defined to characterize $P_\Omega$. A necessary condition for the appearance of a phase transition is that $\hat{F}$ shows two minima as a function of the relevant order parameter. In the Onsager[21] and Maier–Saupe[29] theories of the I–N transition in 3D systems, the $O(\rho^2)$ terms are neglected, and $P_\Omega$ (and hence $\hat{F}$), is expressed in terms of a single order parameter, say $\Delta$, measuring the tendency of the rods to align parallel to each other. It is convenient to define $\Delta$ so that $\Delta = \Delta_I = 0$ for the isotropic distribution $P_\Omega = P^I_\Omega = \text{constant}$; [$P^I(\Omega) = 1/4\pi$ for continuous $\Omega$]. In 3D, $\Delta = \Delta_I = 0$ ($P_\Omega = P^I_\Omega$) corresponds to a minimum of $\hat{F}$ (either global or local) over a wide range of densities. (This is not the case for grafted rods, see below.) The appearance of a nematic phase becomes possible only when $\hat{F}$ shows another minimum at $\Delta = \Delta_N \neq 0$, with coexistence properties ($\rho_I, \rho_N, \Delta_I, \Delta_N$) determined from the usual requirements of equal pressures, $\Pi_I = \Pi_N$, and chemical potentials, $\mu_I = \mu_N$. Recall that $\Pi = \rho^2[\partial(F/N)/\partial\rho]$ and $\mu = F/N + \Pi/\rho$ with $F = F^0 + \hat{F}$ denoting the full free energy.

The 3D rod mixture can exhibit an additional, gas–liquid ($g$–$l$), transition at densities $\rho < \rho_I$. Clearly, at these densities $F = F^0$ [as given by Eq. (17) or the generalized vdW form (9)], since $P_\Omega = P^0_\Omega$ and hence $\hat{F} \equiv 0$. The coexisting densities $\rho_g$ and $\rho_l$ are determined again by $\mu_l = \mu_g$ and $\Pi_l = \Pi_g$. The relevant order parameter of this transition is $\rho$ since the two phases correspond to minima of $G = N\mu$, with their $\rho$ satisfying $\partial G/\partial\rho = 0$. (Note that a $g$–$l$ transition is possible only if $\langle w\rangle^0 < 0$.)

As we shall see below, in the monolayer problem, $P_\Omega$ departs from $P^0_\Omega$, as soon as $\rho$ becomes finite. Hence, even if a $g$–$l$ transition takes place prior to the onset of an orientational transition, $P_\Omega$ is generally different for the two phases, i.e., the change in $\rho$ is coupled to a change in $\Delta$. Furthermore, in some cases the $g$–$l$ and the orientational transition are not separable. We elaborate on this issue in Sec. III C.

Identifying the stable phases by minimizing $\hat{F}$ with respect to $\Delta$ is consistent with the more general requirement that $P_\Omega$ in Eq. (9) [and hence in Eq. (18)] is in fact the most probable orientational pdf. At the minimum of $\hat{F}$ we have $\delta\hat{F} = \Sigma(\partial\hat{F}/\partial P_\Omega)\delta P_\Omega = 0$ for all $\{\delta P_\Omega\}$, subject only to $\Sigma\delta P_\Omega = 0$. Using Eq. (18) we find that $P_\Omega$ must satisfy the self-consistency relation

$$P_\Omega = \frac{1}{Y}P^0_\Omega \exp\left[-\rho\sum_{\Omega'} P_{\Omega'} w_{\Omega\Omega'}\right] \tag{19}$$

with $Y$ determined by the normalization condition $\Sigma P_\Omega = 1$. The exponent in the Boltzmann-like distribution (19), or more precisely

$$\Phi_\Omega = kT\rho\sum_{\Omega'} P_{\Omega'} w_{\Omega\Omega'} \tag{20}$$

can be interpreted as the mean-field potential acting on a rod with orientation $\Omega$. Note from Eq. (14) for $w$ that it contains contributions from both repulsions and attractions.

For rodlike particles in 3D, $w_{\Omega\Omega'}$ depends only on the relative orientation of the two rods, implying that $\Sigma_{\Omega'} w_{\Omega\Omega'}$ is independent of $\Omega$. Consequently, the mean field potential corresponding to the isotropic distribution, $\Phi^I_\Omega = kT\rho\Sigma_{\Omega'} P^I_{\Omega'} w_{\Omega\Omega'}$, is also independent of $\Omega$ (since $P^I_\Omega = \text{constant}$). In the absence of fields [$\epsilon(\Omega) \equiv 0$] $P^0_\Omega = P^I_\Omega$, and hence $P_\Omega = P^I_\Omega$ is a solution of Eq. (19) for all $\rho$. In other words, the isotropic phase corresponds to an extremum of $\hat{F}$ at all densities.

In marked contrast to the 3D case, in the monolayer $\Sigma_{\Omega'} w_{\Omega\Omega'}$, and hence $\Phi^I_\Omega$ (and more generally $\Phi^0_\Omega = kT\rho\Sigma_{\Omega'} P^0_{\Omega'} w_{\Omega\Omega'}$ for cases where $\epsilon(\Omega) \neq 0$) are *not* independent of $\Omega$. This is due to the lower symmetry of the monolayer, resulting from the existence of the impenetrable surface which restricts the allowed rod orientations to one hemisphere ($0 \leqslant \theta \leqslant \pi/2$ as compared to $0 \leqslant \theta \leqslant \pi$ in 3D). This implies that $w_{\Omega\Omega}$ and $\Sigma_{\Omega'} w_{\Omega\Omega'}$ are $\Omega$ dependent, as will be demonstrated for a specific model in the next section. Clearly $P_\Omega = P^0_\Omega$ is a solution of Eq. (19) for $\rho = 0$. But as soon as $\rho$ becomes finite $P^0_\Omega$ can no longer be a solution since $\Phi_\Omega$ is not a constant, and hence $P_\Omega \propto P^0_\Omega \exp[-\beta\Phi_\Omega] \neq P^0_\Omega$. As a special case these conclusions apply also to systems with $\epsilon(\Omega) = 0$, for which $P^0_\Omega = P^I_\Omega$ is the isotropic distribution.

The different symmetry properties of $w_{\Omega\Omega'}$ in the bulk and the monolayer explain additional differences in the phase behavior between the two types of systems. For example, in the 3D case large anisotropy of $w_{\Omega\Omega'}$ (i.e., preference for $\Omega \sim \Omega'$), combined with the fact that $w_{\Omega\Omega'}$ is $\Omega$ independent, suffice to explain the appearance of a stable nematic phase, regardless of the origin of $w_{\Omega\Omega'}$. Thus in Onsager's theory, the I→N transition is accounted for in terms of excluded volume interactions ($w_{\Omega\Omega'} = 2b_{\Omega\Omega'}$ and $a_{\Omega\Omega'} = 0$), whereas in Maier–Saupe's approach $w_{\Omega\Omega'}$ is due entirely to the anisotropic attractive interactions. On the other hand, purely excluded area interactions do *not* induce an orientational transition in the *monolayer*. Such a transition is predicted only if attractive contributions are added to $w_{\Omega\Omega'}$.

Consider now the restricted orientational model described in Sec. II. Suppose that one end of the rod is at the origin of a Cartesian coordinate system. Then in 3D its other end can point into the $\pm x$, $\pm y$, or $\pm z$ directions. For symmetric rods the $\pm x$ (and similarly the $\pm y$ and $\pm z$) orientations are indistinguishable, reducing the number of orientations to three, $\Omega = x,y,z$. In the monolayer problem, the surface is the $xy$ plane and the $-z$ direction is forbidden. While in 3D the isotropic distribution is naturally $P_x^{\mathrm{I}} = P_y^{\mathrm{I}} = P_z^{\mathrm{I}} = 1/3$, for grafted rods the identification of $P_\Omega^{\mathrm{I}}$ is not as obvious. We take here $P_\Omega^{\mathrm{I}} = 1/3$ for $\Omega = x,y,z$ (corresponding to $P_x^{\mathrm{I}} = P_{-x}^{\mathrm{I}} = P_y = P_{-y} = 1/6$ and $P_z^{\mathrm{I}} = 1/3$), because for this $P_\Omega^{\mathrm{I}}$ the usual orientational order parameter, namely $\langle P_2(\cos\theta)\rangle$ vanishes (as in 3D); $P_2(\cos\theta) = (3\cos^2\theta - 1)/2$ is the second Legendre polynomial. As we shall see below the basic qualitative characteristics of the monolayer phase behavior are independent of what we take for $P_\Omega^{\mathrm{I}}$. A more relevant quantity is the zero density distribution $P_\Omega^0 \sim P_\Omega^{\mathrm{I}} \exp[-\beta\epsilon(\Omega)]$. More specifically, for the restricted orientational model ($\Omega = x,y,z$) the fraction of rods, which at $\rho \to 0$ lie down on the surface ("$s$" $= x$ or $y$) is $P_s^0 = P_x^0 + P_y^0$ and the fraction of upright ($z$) rods $P_z^0 = 1 - (P_x^0 + P_y^0) \equiv 1 - P_s^0$ are related to the adsorption energy via

$$\ln(P_s^0/2P_z^0) = (\chi - 1)\epsilon. \tag{21}$$

The matrix of excluded areas ($2b_{\Omega\Omega'}$, with $\Omega,\Omega' = x,y,z$) corresponding to the restricted orientational model, for rectangular parallelepipeds, is easily shown to be

$$\mathbf{b} = \begin{bmatrix} 2\chi & \frac{1}{2}(\chi+1)^2 & (\chi+1) \\ \frac{1}{2}(\chi+1)^2 & 2\chi & (\chi+1) \\ (\chi+1) & (\chi+1) & 2 \end{bmatrix}. \tag{22}$$

This matrix should be contrasted with the corresponding matrix of excluded volumes, $2\mathbf{b}^{(3D)}$, for the same rod model in 3D: In the bulk case all the diagonal elements are equal and likewise the nondiagonal elements. Specifically,

$$b_{\Omega\Omega'}^{(3D)} = \begin{cases} 4\chi & \Omega = \Omega' \\ (\chi+1)^2 & \Omega \neq \Omega' \end{cases}. \tag{23}$$

In the monolayer this full symmetry is seen to be broken due to the difference between in-plane ($x,y$) and upright ($z$) rods. Note in particular that $2b_{zz} = 4$ is the smallest excluded area, indicating the tendency of the rods to stand up as $\rho = N/A$ increases.

For rods in 2D the matrix of excluded area $\mathbf{b}^{(2D)}$ consists of the $2\times 2$ in-plane ($x,y$) minor of Eq. (22). Here, like in the bulk case, the diagonal elements of $\mathbf{b}$ are equal. Thus the monolayer, which is neither a 2D nor a 3D system, is characterized by a lower symmetry as compared to either of these cases.

The attractive part, $a_{\Omega\Omega'}$, of the interaction matrix $w_{\Omega\Omega'}$ depends on $u_a$, cf. Eq. (8). To calculate $a_{\Omega\Omega'}$ we treat the rod as a row of $\chi$ segments ("atoms") placed (either horizontally or vertically) on a square lattice, with unit lattice constant, as described in Sec. II. The attractive interaction between neighboring rods is taken as a sum of nearest-neighbor segment–segment potentials, see Eq. (4). For this model the integration in Eq. (8) corresponds to "moving" an $\Omega$ rod around an $\Omega'$ rod. Using Eq. (4) in Eq. (8) we find, for example, that $\beta a_{xx} = \beta a_{yy} = u(\chi^2 + 1)$, quite different from $\beta a_{zz} = 2u\chi$. To allow for still larger asymmetry (as may be the case in surfactant monolayers) we shall write $a_{zz} = 2u\chi\alpha$ and examine some cases with $\alpha \neq 1$. The full $a_{\Omega\Omega'}$ matrix is found to be

$$\beta\mathbf{a} = u\begin{bmatrix} (\chi^2+1) & 2\chi & (\chi+1) \\ 2\chi & (\chi^2+1) & (\chi+1) \\ (\chi+1) & (\chi+1) & 2\chi\alpha \end{bmatrix}. \tag{24}$$

For the 3D case the same model yields

$$\beta a_{\Omega\Omega'}^{(3D)}/u = \begin{cases} 2\chi^2 + 1 & \Omega = \Omega' \\ \chi(\chi+2) & \Omega \neq \Omega' \end{cases}. \tag{25}$$

For rods in the plane $\beta\mathbf{a}^{(2D)}$ is given by the $x,y$ minor of Eq. (24). Thus, as with $\mathbf{b}$, for the pure 2D and 3D cases the diagonal elements of $\mathbf{a}$ are equal whereas in the monolayer $a_{xx} = a_{yy} \neq a_{zz}$. This lower ("broken") symmetry will be reflected in the phase behavior of the monolayer as we shall see below.

### B. The standing up ($s$–$z$) transition

From Eq. (22) we see that excluded area interactions tend to increase the fraction, $P_z$, of standing rods, thus reducing the fraction $P_s = P_x + P_y = 1 - P_z$ of surface rods. In the $xy$ plane the interactions tend to align the rods parallel to each other, an effect which is enhanced by the attractive interactions, cf. Eq. (24). These two tendencies may induce two types of ordering transitions: A standing up (or "$s$–$z$") transition associated with a change in $P_z = 1 - P_s$, and an in-plane (or "$x$–$y$") I–N transition involving a change in $q_x = P_x/(P_x + P_y) = P_x/P_s$ and $q_y = P_y/P_s = 1 - q_x$, the proportion of rods lying along the $x$ and $y$ axes, respectively.

Using the definitions of $P_s$, $P_z$, $q_x$, and $q_y$, the orientational free energy for the three-state model can be expressed as a sum of two terms

$$\hat{F} = F_{sz} + P_s F_{xy}, \tag{26}$$

in which $F_{sz}$ and $F_{xy}$ are the free energies corresponding to the two types of transitions mentioned above. Explicitly

$$\beta F_{sz}/N = P_z \ln(P_z/P_z^0) + P_s \ln(P_s/P_s^0) + \tfrac{1}{2}\rho[P_z^2 w_{zz} + 2P_z P_s w_{zs} + P_s^2 w_{ss} - \langle w\rangle^0], \tag{27}$$

where $\langle w\rangle^0 = (P_z^0)^2 w_{zz} + 2P_z^0 P_s^0 w_{zs} + (P_s^0)^2 w_{ss}$. $w_{ss}$ is the isotropic ($q_x = q_y = 1/2$) average of the rod–rod interaction in the $xy$ plane:

$$w_{ss} = (w_{xx} + w_{yy} + 2w_{xy})/4 = (w_{xx} + w_{xy})/2. \tag{28}$$

Introducing an orientational order parameter $\Delta$,

$$\Delta = P_z - P_z^0 = P_s^0 - P_s, \tag{29}$$

we can rewrite Eq. (27) as

$$\beta F_{sz}/N = (P_z^0 + \Delta)\ln(1 + \Delta/P_z^0) + (P_s^0 - \Delta)\ln(1 - \Delta/P_s^0) - \rho V\Delta + \tfrac{1}{2}\rho W\Delta^2, \tag{30}$$

where it should be noted that $-P_z^0 \leqslant \Delta \leqslant P_s^0$. $V$ and $W$ are defined as

$$V = P_z^0(w_{zs} - w_{zz}) + P_s^0(w_{ss} - w_{zs}), \tag{31}$$

$$W = w_{zz} + w_{ss} - 2w_{zs}. \tag{32}$$

The order parameter $\Delta$ measures the excess fraction of $z$ rods, as compared to their fraction at $\rho = 0$. Of course, other quantities, e.g., $P_z$, could also serve as order parameters.

For the free energy of the surface rods we have

$$\beta F_{xy}/N = q_x \ln q_x + q_y \ln q_y + \ln 2 + \tfrac{1}{2}\rho P_s [q_x^2 W_{xx} + 2q_x q_y w_{xy} + q_y^2 w_{yy} - w_{ss}]. \tag{33}$$

Note that $F_{xy} = 0$ for the isotropic 2D distribution $q_x^0 = q_y^0 = 1/2$ (which is also the equilibrium distribution at $\rho = 0$).

Introducing, in analogy to Eq. (29), an in-plane order parameter $\eta = q_x - 1/2 = q_y + 1/2$, we find (using $w_{xx} = w_{yy}$)

$$\beta F_{xy}/N = (1/2 + \eta)\ln(1 + 2\eta) + (1/2 - \eta) \times \ln(1 - 2\eta) + \tfrac{1}{2}\rho_s \eta^2 W_s, \tag{34}$$

with $\rho_s = P_s\rho = (P_s^0 - \Delta)\rho$ denoting the (2D) number density of surface rods, and

$$W_s = w_{xx} + w_{yy} - 2w_{xy} = 2(w_{xx} - w_{xy}) \tag{35}$$

denoting the net interaction potential between surface rods. Unlike $F_{sz}$, the 2D free energy $F_{xy}$ does not contain a linear term in the order parameter. This is due to the symmetry $w_{xx} = w_{yy}$, as opposed to the $w_{zz} \neq w_{ss}$ asymmetry in $F_{sz}$.

Both $F_{sz}$, as given by Eq. (27) or Eq. (30), and $F_{xy}$, as given by Eq. (33) or Eq. (34), correspond to mean-field (Bragg–Williams) free energies of two-state systems. In particular $F_{xy}$, with appropriate identification of the interaction parameter $\rho_s W_s$, is completely analogous to the free energy of a binary solution (or lattice gas or spin 1/2) system.[30] Similarly, $F_{sz}$ is similar to the free energy of an asymmetric ($w_{zz} \neq w_{ss}$) binary system (or a system in a field). Thus many characteristics of the standing-up and the in-plane transitions can be inferred by analogy to the corresponding binary systems. In the monolayer problem the two transitions are coupled to each other through $P_s$, which appears in Eq. (27) (as the order parameter) and in Eq. (33) (as a parameter measuring the interaction strength). Both transitions are coupled to the $g$–$l$ transition. These couplings were first discussed by Boehm and Martire[16] and later treated by Chen *et al.*[18] and analyzed in detail by Wang.[19] We shall briefly discuss the role of the in-plane ($x$–$y$) ordering in the context of the Monte Carlo simulations presented in Sec. IV. However, our main interest in this paper is in the standing-up transition, its different features as compared to the I–N transition in 3D and its coupling to the gas–liquid transition. Therefore, our mean-field analysis of $F$ will focus on $F_{sz}$, to which end we shall assume $F_{xy} = 0$. This suppression of the in-plane free energy corresponds to assuming that the rod orientational distribution on the surface is always isotropic: $q_x = q_y = 1/2$. This is rigorously true for a somewhat different model system in which, on the surface, the particles are isotropic (e.g., squares or circles) rather than rodlike. For example, large squares can be used to represent lying-down particles with small squares used for standing-up ones. The free energy of such a system is also given by Eq. (27) or Eq. (30) (with $s$ and $z$ corresponding to large and small particles). Some MC simulations for this system of bidisperse interconverting squares are presented in Sec. IV.

Differentiating Eq. (30) we find the extremum condition for $F_{sz}$,

$$(\beta/N)\frac{\partial F_{sz}}{\partial \Delta} = \ln\left(\frac{1 + \Delta/P_z^0}{1 - \Delta/P_s^0}\right) + \rho(W\Delta - V) = 0. \tag{36}$$

The next two derivatives are given by

$$(\beta/N)\frac{\partial^2 F_{sz}}{\partial \Delta^2} = \frac{1}{P_z^0 + \Delta} + \frac{1}{P_s^0 - \Delta} + \rho W, \tag{37}$$

$$(\beta/N)\frac{\partial^3 \hat{F}_{sz}}{\partial \Delta^3} = -\frac{1}{(P_z^0 + \Delta)^2} + \frac{1}{(P_s^0 - \Delta)^2}. \tag{38}$$

Explicit expressions for $W$ and $V$ for our rod–rod interaction model are obtained from Eqs. (14), (22–25), (28), (31), and (32). For the monolayer we get

$$W = \tfrac{1}{2}(\chi - 1)^2 - u[(\chi - 1)(\chi + 3) + 4\chi(a - 1)], \tag{39}$$

$$V = 2P_z^0(\chi - 1) + (P_s^0/2)(\chi - 1)(\chi + 3) - u[2P_z^0(2a\chi - \chi - 1) + P_s^0(\chi^2 - 1)], \tag{40}$$

and for the bulk case

$$W^{(3D)} = -(3/2)(\chi - 1)^2(1 + u); \quad V^{(3D)} = 0. \tag{41}$$

Since $V^{(3D)} = 0$ the isotropic solution $\Delta = 0$ satisfies Eq. (36) for all $\rho$. On the other hand, in the monolayer one generally has $V \neq 0$, and hence $\Delta = 0$ is a minimum of $F_{sz}$ only when $\rho \to 0$, consistent with our general conclusion based on Eqs. (19), and (20). For both the monolayer and the bulk cases, at sufficiently low densities, $\partial^2 F_{sz}/\partial \Delta^2 > 0$, implying that the low density solution is indeed a minimum of $F_{sz}$. [In the bulk case $W^{(3D)}$ is always negative, and $\Delta = 0$ turns into a maximum at high $\rho$].

A necessary condition for the appearance of a first order orientational transition is that $F_{sz}$ should obtain two minima, say at $\Delta_1$ and $\Delta_2$. Thus at some $\Delta = \Delta_m$ ($\Delta_1 < \Delta_m < \Delta_2$) $F_{sz}$ must have a maximum, at which point $\partial^2 F_{sz}/\partial \Delta^2 < 0$. This condition can only be fulfilled if $W < 0$ and $|\rho W|$ is large enough to overcome the first two (entropic) terms in Eq. (37). From Eq. (41) we see that this requirement is easily satisfied in the bulk case (especially for large $\chi$), where $W^{(3D)} < 0$ and $|\rho W|$ increases with $\rho$ and $u$ (recall $u \sim 1/T$). Note that $W^{(3D)} < 0$ regardless of whether the interaction is dominated by excluded volume repulsion [as in Onsager's or Zwanzig's theories which correspond to $u = 0$ in Eq. (41)] or by an attractive potential (as in Maier–Saupe's theory).

On the other hand, from Eq. (39) we see that in the layer case $W$ can be either positive or negative, depending on

whether the interaction is dominated by the repulsive or attractive parts of the potential, respectively. In particular, for hard rods ($u \equiv 0$) we always find $W > 0$, implying—in contrast to the bulk case—that a monolayer of *hard rods* cannot exhibit an orientational phase transition. A similar conclusion has been reached by Halperin *et al.*[17] based on a monolayer version of Onsager's theory[21] of the I–N transition, and by Chen *et al.*[18] based on a Landau analysis of the monolayer version of Zwanzig's three-state model. It should be stressed that our conclusion that hard rods ($u \equiv 0$) do not show a first order transition is independent of the adsorption energy $\epsilon$.

In a monolayer of hard rods the equilibrium order parameter $\Delta = \Delta_1$, corresponding to the single minimum of $F_{sz}$, increases monotonically with $\rho$. Figure 1 shows $P_z = P_z^0 + \Delta$ as a function of $\rho$ for hard rods of axial ratio $\chi = 4$ with $\epsilon = 0$ and 1, and for rods with $\chi = 6$, $\epsilon = 0$. The continuous curves were obtained by numerical solution of Eq. (36). It should be noted that for some values of $\rho$ and $\epsilon$ the solution of Eq. (36) yields physically unacceptable solutions for $\Delta$. An acceptable solution is one which satisfies the requirement $\phi < 1$ where

$$\phi = \rho[\chi P_s + P_z] = \rho[1 + (\chi - 1)(P_s^0 - \Delta)] \quad (42)$$

is the coverage (area fraction) of rods on the surface. For large values of $\epsilon$ (and $\chi$) $\phi$ reaches 1 much faster than $\rho$. This is the case, for example, for the curve corresponding to $\chi = 4$, $\epsilon = 1$ in Fig. 1. In this system $\phi \to 1$ when $\rho \to \bar{\rho} \simeq 0.35$. In such cases we assume that for all $\rho > \bar{\rho}$ the coverage $\phi$ remains 1, implying that $\Delta$ increases with $\rho$ according to

$$\Delta = P_s^0 - (1 - \rho)/\rho(\chi - 1). \quad (43)$$

The change in slope of $P_z(\rho) = P_z^0 + \Delta(\rho)$ at $\bar{\rho} \cong 0.35$ in the $\chi = 4, \epsilon = 1$ curve of Fig. 1 is due to switching from Eq. (36) to Eq. (43).

Figure 1 shows also the results obtained for $\Delta_1(\rho)$ from a MC simulation (see Sec. IV below), revealing similar qualitative behavior, and satisfactory quantitative agreement with the mean-field results. Figure 2 shows a comparison between mean-field and simulation results for the chemical potential of hard rods with $\chi = 4$ and $\epsilon = 0$. Again the qualitative behavior is similar and the quantitative agreement is reasonable.

The $\rho$ dependence of $\Delta_i(\rho)$, the order parameter corresponding to branch $i$ of $\partial F_{sz}/\partial \Delta = 0$ is governed by

$$\frac{\partial \Delta_i}{\partial \rho} = -\left[\frac{(\partial^2 F_{sz}/\partial \rho \partial \Delta)}{(\partial^2 F_{sz}/\partial \Delta^2)}\right]_{\Delta = \Delta_i} = \frac{(V - W\Delta_i)}{(\partial^2 F_{sz}/\partial \Delta^2)_{\Delta = \Delta_i}}. \quad (44)$$

[The second equality also follows directly from the $\rho$ derivative of Eq. (36).] For the layer of hard rods [$u = 0$, single branch $\Delta_1(\rho)$] it is easily found using Eqs. (37), (39), and (40) that $\partial \Delta_1/\partial \rho > 0$ for all $-P_z^0 \leqslant \Delta_1 \leqslant P_s^0$, consistent with the results of Fig. 1.

If rod–rod attraction is strong enough, corresponding to large $u$ in Eq. (39), $W$ can become negative, and if $|\rho W|$ is sufficiently large $F_{sz}$ can exhibit two minima and a maximum, signaling the appearance of an orientational phase transition. The three extremum points coincide at a critical point which can be specified by $\Delta = \Delta_c, \rho = \rho_c$, and $u = u_c$. (Recall that $ukT$ is the energy of segment–segment attraction, thus $u_c \sim 1/T_c$.) Near the critical point $\partial F_{sz}/\partial \Delta \sim (\Delta - \Delta_c)^3$. Equivalently, at the critical point the first three derivatives of $F_{sz}$ must vanish,

$$\left(\frac{\partial^k F_{sz}}{\partial \Delta^k}\right)_{\Delta_c \rho_c u_c} = 0 \quad k = 1,2,3. \quad (45)$$

Explicit expressions for the critical constants are ob-

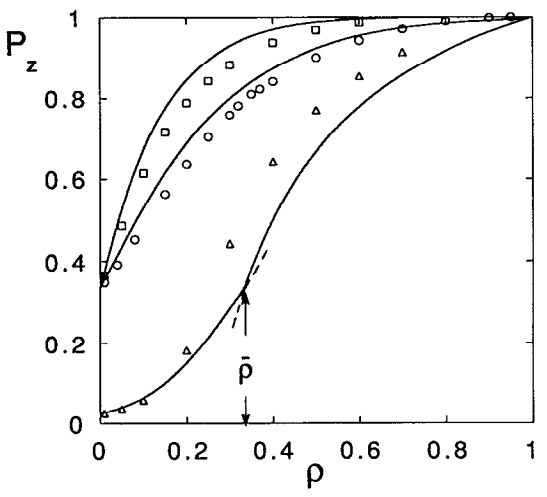


FIG. 1. The fraction of rods in upright ($z$) orientation as a function of surface density in a monolayer of hard rods. The solid curves are the mean-field results corresponding from top to bottom, to $\chi = 6, \epsilon = 0$; $\chi = 4, \epsilon = 0$; and $\chi = 4, \epsilon = 1$. The squares, circles, and triangles show the results of Monte Carlo simulations for these systems, respectively. The change in slope in the mean-field calculation for the last case (of strong adsorption) $\chi = 4, \epsilon = 1$, takes place at the density $\bar{\rho} \cong 0.33$ where the full surface coverage first appears (see the text).

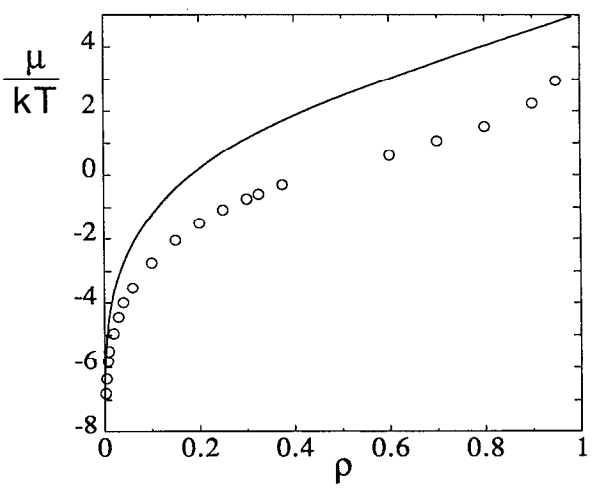


FIG. 2. Chemical potential as a function of density in a monolayer of hard rods with $\chi = 4$ and $\epsilon = 0$. Solid curve—mean field calculation. Circles—computer simulations.

tained using Eqs. (36)–(38) for the derivatives, and Eqs. (39) and (40) for $W$ and $V$. For $\Delta_c$ we get immediately

$$\Delta_c = 1/2 - P_z^0 = P_s^0 - 1/2, \tag{46}$$

which corresponds to $P_z^c = P_z^0 + \Delta_c = P_s^c = 1/2$, i.e., at the critical point half of the rods are standing up and the other half lie down on the surface.

To simplify somewhat the expressions for $\rho_c$ and $u_c$ let $W_a$ and $W_r$ denote, respectively, the attractive and repulsive components of $W$, cf. Eq. (39). That is, we write $W = W_r - uW_a$ with $W_r = (\chi - 1)^2/2$ and $W_a = [(\chi - 1)(\chi + 3) + 4\chi(\alpha - 1)]$. Similarly, we write Eq. (40) as $V = V_r - uV_a$. Then, after some algebra, we find

$$u_c = \frac{hW_r + V_r}{hW_a + V_a} \tag{47}$$

with $h = h(P_z^0) = [\ln(P_s^0/P_z^0) - 2(P_s^0 - P_z^0)]/4$. For $\rho_c$ we get

$$\rho_c = 4/[u_c W_a - W_r] = c + d\epsilon. \tag{48}$$

Here $c = c_1/c_2$ and $d = (\chi - 1)W_a/c_2$ with $c_1 = 4[(\chi - 1)^2 - 4\chi(\alpha - 1)] + W_a \ln 2$ and $c_2 = [\chi^3(2\alpha + 1) + \chi^2(4\alpha - 5) - \chi(6\alpha + 1) + 5]$. $\epsilon$ is the segment adsorption energy, cf. (21).

Figure 3 shows how $1/u_c (\sim T_c)$ varies with $\epsilon$ for ($\chi$, $\alpha$) = (4, 1), (6, 1), (10, 1), and (4,2). Each curve divides the $u$, $\epsilon$ plane into two regions: Above and to the left of the curve $\Delta$ changes continuously with $\rho$ at all densities. For all $u$, $\epsilon$ points below and to the right of the curve, there is a certain density $\tilde{\rho} = \rho(\epsilon, u)$, such that for $\rho < \tilde{\rho}$ $F_{sz}(\Delta)$ shows a single minimum [at $\Delta_1 = \Delta_1(\rho)$]; at densities $\rho > \tilde{\rho}$ $F_{sz}(\Delta)$ develops two minima, at $\Delta_1(\rho)$ and $\Delta_2(\rho)$, signaling the possibility of a first order orientational transition (see below).

Since at the critical point $P_z^c = P_s^c = 1/2$, the critical coverage is $\phi_c = \rho_c(P_z^c + P_s^c\chi) = (\chi + 1)\rho_c/2$. Figure 4 shows how $\phi_c$ varies with $\epsilon$, for the same values of $\chi$ and $\alpha$ considered in Fig. 3. The increase of $\rho_c$ with $\epsilon$ reflects the increasing reluctance of the rods to undergo a standing-up transition at higher adsorption energies. Since $u_c$ decreases as $\rho_c$ increases, see Eq. (48), larger $\epsilon$ implies lower $u_c$, as confirmed by Fig. 3.

Figure 5 shows $\Delta_1(\rho)$ and $\Delta_2(\rho)$, the two branches of minima of $F_{sz}(\Delta)$ characteristic of systems at $T < T_c$, for a

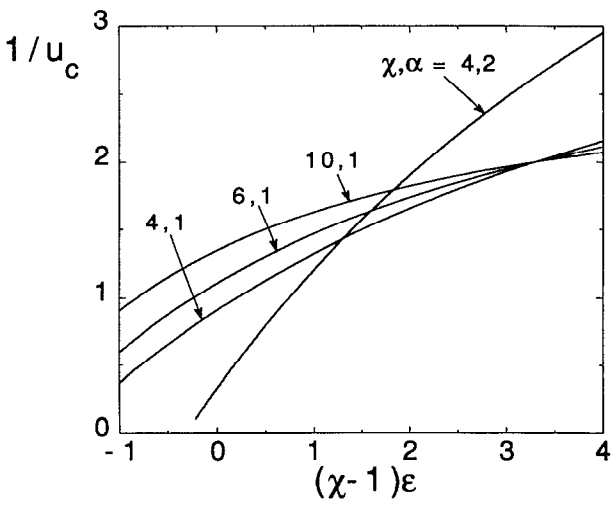


FIG. 3. Critical temperature ($T_c \sim 1/u_c$, see the text) as a function of adsorption energy for four representative systems.

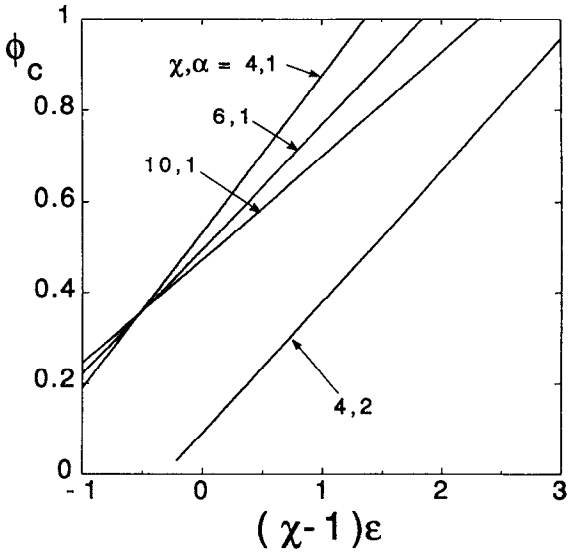


FIG. 4. Critical area fraction as a function of adsorption energy for the four representative monolayers from Fig. 3.

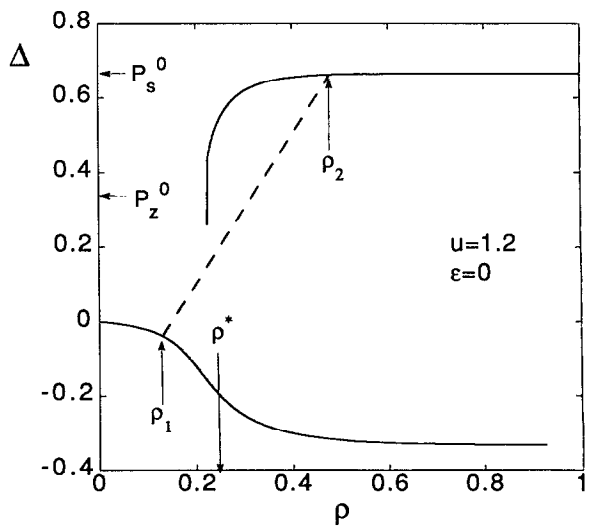


FIG. 5. Orientational order parameter as a function of surface density for a monolayer of rods with $\chi = 4$, $\alpha = 1$ and adsorption energy $\epsilon = 0$ ($P_z^0 = 1/3$). For this system $u_c$ ($\sim 1/T_c$) = 1.109. The results shown are for $u = 1.2$, i.e., $T/T_c = u/u_c \cong 0.92$. For this system a second branch of minima of $F_{sz}$ sets in at $\rho \cong 0.22$. At $\rho^* \simeq 0.244$ the two minima are of equal depth. $\rho_1$ and $\rho_2$ mark the densities (and $\Delta_1$ and $\Delta_2$ the order parameters) of the coexisting phases, as obtained by solving Eqs. (49) and (50), see the text. The system considered here shows only one first-order phase transition.

monolayer of rods with $\chi = 4, \epsilon = 0, \alpha = 1$. For this case we find from Eq. (47) that $u_c = 1.109$ so that $T/T_c = u_c/u = 0.92$. It is clearly seen that a second, high $\Delta$, branch appears at $\rho \gtrsim \tilde{\rho} \simeq 0.22$. For the same system we show in Fig. 6 how $\Delta = \Delta(u_c)$ changes along the critical isotherm.

In the mean-field equations (30) and (36)–(38) all the interaction terms are multiplied by $\rho$, which can thus be regarded as a coupling constant measuring the strength of the interaction. As noted earlier, $F_{sz}$ as given by Eq. (27) or Eq. (30), is very similar to the free energy (in the Bragg–Williams approximation) of a binary mixture described by a lattice model with nearest-neighbor interactions. This analogy can be stretched further by assuming that each lattice site is occupied either by an $s$ rod or a $z$ rod (but no vacancies) and the nearest-neighbor interactions are proportional to $\rho w_{ss}, \rho w_{sz}$, and $\rho w_{zz}$. Since all sites are occupied by particles, this system is assumed to be uniformly dense even if phase separation takes place. In other words, this scheme ignores "$\Pi A$" effects, (Recall, however, that our $w_{ij}$'s include the effects of excluded area interactions). In this approximation a first order phase transition takes place when the two minima of $F_{sz}$ are equal, $F_{sz}(\Delta_1) = F_{sz}(\Delta_2)$. For the example considered in Fig. 5 this condition is met when $\rho = \rho^* \simeq 0.244$.

The density change accompanying the jump in $\Delta$ in the course of the orientational transition is determined by the requirement of equal pressures, $\Pi$, and chemical potentials, $\mu$, of the coexisting phases. Let $\Pi_i(\rho) = \Pi[\rho, \Delta_i(\rho)]$ and $\mu_i(\rho) = \mu[\rho, \Delta_i(\rho)]$ denote the pressure and chemical potential along branch $i$ ($i = 1,2$). Then, the densities $\rho_1$ and $\rho_2$ and the order parameters $\Delta_1(\rho_1)$, $\Delta_2(\rho_2)$, of the coexisting phases are determined by

$$\Pi[\rho_1, \Delta_1(\rho_1)] = \Pi[\rho_2, \Delta_2(\rho_2)], \tag{49}$$

$$\mu[\rho_1, \Delta_1(\rho_1)] = \mu[\rho_2, \Delta_2(\rho_2)]. \tag{50}$$

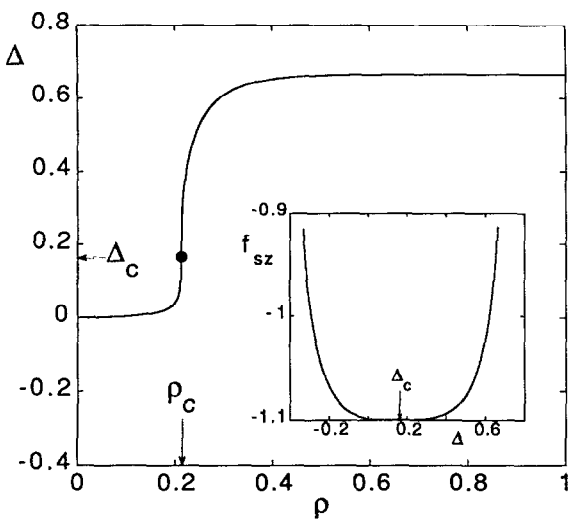


FIG. 6. Critical isotherm of the orientational order parameter vs density. The results are shown for the same system ($\chi = 4, \alpha = 1, \epsilon = 0$) considered in Fig. 5, for which $u_c = 1.109$. $\Delta_c = 1/2 - P_2^0 = 1/6$.

The solution of these equations for $\chi = 4, \alpha = 1, \epsilon = 0$, and $u = 1.2$, as shown in Fig. 5 yield $\rho_1 = 0.13$, $\Delta_1 = -0.04$, and $\rho_2 = 0.48$, $\Delta_2 = 0.66$. The change in area fraction is smaller than in $\rho$, namely $\phi_1 \simeq 0.4$, $\phi_2 \cong \rho_2 = 0.48$. In solving Eqs. (49) and (50), we have used the generalized van der Waals free energy with $\Delta_i$ determined by minimization of $F_{sz}$. [A qualitatively similar behavior, though for different interaction potentials was found by Wang[19] for longer, $\chi = 10$, rods, using the full generalized vdW equation (9) for analyzing the orientational transition]. We elaborate on this point in the next section where we discuss the relation between the orientational and the gas–liquid transitions.

### C. Successive transitions

In addition to the standing-up ($s$–$z$) transition discussed in the previous section, the monolayer can exhibit a gas–liquid ($g$–$l$) transition. The distinction between the two transitions is somewhat subtle since they both involve changes in $\Delta$ and in $\rho$. However, as noted in Sec. III B, the hierarchy of these variables in the two transitions is different. $\Delta$ is the order parameter of the orientational transition, with $\rho$ accompanying the change in $\Delta$ so as to ensure equality of $\Pi$ and $\mu$ of the coexisting phases. On the other hand, $\rho$ is the order parameter of the gas–liquid transition, with $\Delta = \Delta(\rho)$ adjusting so as to minimize the system's free energy at any density. Physically, the orientational transition is driven by the anisotropy of the interaction potential as measured by the interaction parameters $W$ and $V$, whereas the gas–liquid transition is dominated by the isotropic part (or, more precisely, the average) of the interaction potential, e.g., $\langle w \rangle^0$ in Eq. (17).

The phase behavior of the monolayer is determined by an interplay between the molecular parameters $\chi$, $\alpha$, $u$, and $\epsilon$. For some combinations of these parameters the monolayer at low temperatures shows only one first-order phase transition. More interesting systems are those in which, at a certain temperature regime, the $\Pi$–$\rho$ isotherms exhibit two flat portions, one between $\rho_g$ and $\rho_l$ and the other between $\rho_1$ and $\rho_2$, corresponding, respectively, to successive $g$–$l$ and $s$–$z$ transitions ($\rho_g < \rho_l < \rho_1 < \rho_2$). The coexistence curves (or $T$–$\rho$ diagrams) of such monolayers are typically characterized by two humps, which end at critical points $\rho_c^{g-l}, T_c^{g-l}$ and $\rho_c^{s-z}, T_c^{s-z}$ and intersect at a triple point $\rho_{tp}$, $T_{tp}$, with $\rho_c^{g-l} < \rho_{tp} < \rho_c^{s-z}$ and $T_{tp} < T_c^{g-l}, T_c^{s-z}$. Let us assume, as in most cases of interest that $T_c^{g-l} < T_c^{s-z}$. Then, isothermal compression at $T > T_c^{s-z}$ results in continuous increase in $\Delta = \Delta(\rho)$, similar to that of hard rods. If $T_c^{s-z} > T > T_c^{g-l}$ the monolayer will exhibit one first-order, standing-up, transition at high densities. At $T < T_{tp}$ the system transforms directly from the gas to the higher density ($z$) phase of the $s$–$z$ transition. Finally, as demonstrated for a specific system in Fig. 7, when $T_{tp} < T < T_c^{g-l}, T_c^{s-z}$ the monolayer undergoes two successive phase transitions. Here, the gas–liquid ($g$–$l$) and the standing-up ($s$–$z$) transitions of the grafted rod layer are analogous to the gas–liquid-expanded ($g$–$le$) and liquid-expanded–liquid-condensed ($le$–$lc$) transitions in surfactant monolayers. Clearly then, the lower density ($s$) phase in the

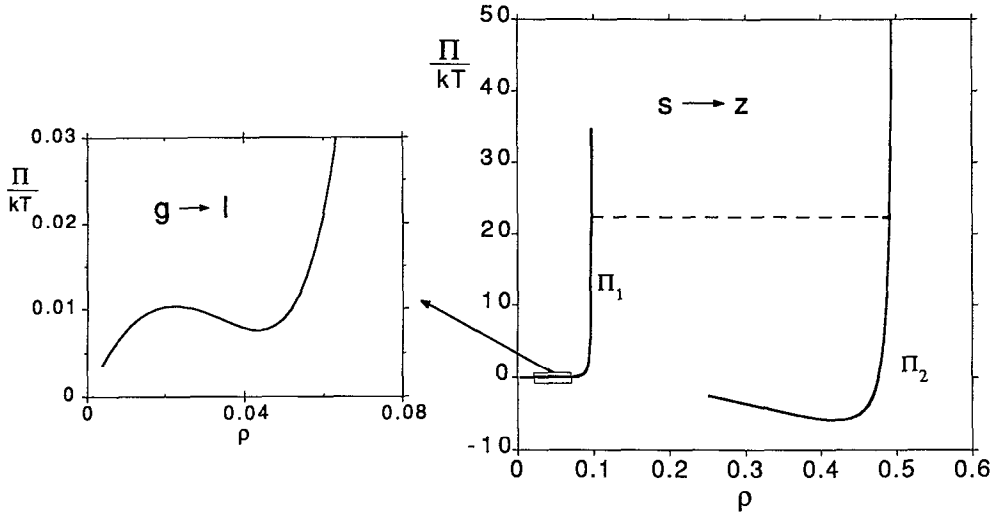


FIG. 7. Pressure($\Pi$)–density($\rho$) isotherm for a system with $\chi = 4$, $\epsilon = 4/3$, and $\alpha = 2$ at $u = 3$. Two first-order phase transitions occur, a gas–liquid, ($g \rightarrow l$) transition at very low density (left) and a standing-up, ($s \rightarrow z$) transition between condensed phases (see the text). The dashed line ties the coexisting phases.

$s$–$z$ transition and the liquid phase ($l$) in the $g$–$l$ transition are the same, corresponding to the *le* phase in surfactant systems. In the next section this correspondence is demonstrated by computer simulations. In the mean-field analysis it is reflected by the fact that the $l$ and $s$ phases belong to the same pressure branch, $\Pi_1$.

A possible approximate scheme for analyzing the sequence of monolayer transitions would be to use the vdW equation (15) with the low density coefficients $\langle b \rangle = \langle b \rangle^0$ and $\langle a \rangle = \langle a \rangle^0$ for the $g$–$l$ transition, and $F_{sz}$ from Eq. (30) for the $s$–$z$ transition. Then, if the vdW pressure loop is completed before the standing-up transition sets in, as shown by the appearance of a second branch of $F_{sz}$, the conclusion would be that the transitions are separate. Note, however, that in this vdW equation $P_\Omega = P_\Omega^0$ is constant ($\Delta \equiv 0$) before and throughout the $g$–$l$ transition. As discussed in previous sections, this assumption is valid for bulk systems and may turn out as an adequate approximation for some monolayers (with large $\epsilon$). Yet, it ignores one of the most unique characteristics of the monolayer, namely, the continuous variation of $P_\Omega$ with $\rho$ which begins as soon as $\rho$ becomes finite.

In order to account for the change of $\Delta$ with $\rho$ along a $g$–$l$ isotherm, we use Eq. (15) with the density dependent coefficients $\langle b \rangle = b(\Delta)$ and $\langle a \rangle = a(\Delta)$ to calculate $\Pi$. Similarly, we calculate $\mu = F/N + \Pi/\rho$ using $F$ from Eq. (6). The $\rho$ dependences of $\langle a \rangle$ and $\langle b \rangle$ enter through the variation of $\Delta$ with $\rho$, which we determine from the minimization of $F_{sz}$. That is, we calculate $b(\Delta) = (P_s^0 - \Delta)(b_{xx} + b_{xy})/2 + (P_z^0 + \Delta) b_{zz}$ [and similarly $a(\Delta)$] using the $\Delta$'s which solve $\partial F_{sz}/\partial \Delta = 0$ with $F_{sz}$ from Eq. (30). Determining $\Delta$ by minimization of $F_{sz}$ rather than $F$ is clearly an approximation since $F_{sz}$ does not account for the entire $\Delta$ dependence of the free energy. However, this approximation captures all the essential physics of the problem.

Corresponding to each branch $\Delta_i(\rho)$ of $F_{sz}$ we obtain an equation of state, $\Pi_i = \Pi_i[\rho, \Delta_i(\rho)] = \Pi_i(\rho)$ from Eq. (15). Similarly, we can calculate the chemical potential along this branch, $\mu_i = \mu_i[\rho, \Delta_i(\rho)] = \mu_i(\rho)$. As we have seen in the previous section, only one branch exists [$\Delta_1(\rho)$] at low densities. In the mean-field picture a gas–liquid transition is recognized by a (vdW) loop of $\Pi_1(\rho)$. This happens when $T < T_c^{g-l}$, i.e., when *on the average* rod–rod attractions [as measured by $a(\Delta)$] are strong enough. $\rho_g$ and $\rho_l$, and hence $\Delta_g$ and $\Delta_l$, are determined by Maxwell construction. A second branch, $\Delta_2(\rho)$, appears at higher densities, provided the *anisotropic* rod–rod attractions, as measured by $W$, are strong enough to ensure $T < T_c^{s-z}$. Then an $s$–$z$ transition can take place between two (expanded and condensed) liquid phases whose densities $\rho_1, \rho_2$, and order parameters $\Delta_1$, $\Delta_2$ at coexistence are determined by solving $\Pi_1 = \Pi_2$ and $\mu_1 = \mu_2$.

It may be noted that for a monolayer of rods (or flexible molecules) with many possible orientations (conformations), the (functional) minimization of $F$ with respect to $P_\Omega$ may result in a vdW-like pressure loop. Thus the orientational transition is indicated by a second loop at high $\rho$, as was found by McIlroy and Cantor for a monolayer of flexible chains.[10] This behavior indicates a continuous passage from one branch to another through a series of local free energy minima, including a nonphysical regime.

If, for $T < T_c^{g-l}$, $T_c^{s-z}$, the calculation above yields $\rho_l < \rho_1$, we conclude that the $g$–$l$ and $s$–$z$ transitions take place successively, as for the system in Fig. 7. This also means that $T > T_{tp}$. At lower temperatures ($T < T_{tp}$) the calculation yields $\rho_1 < \rho_l$, suggesting that the $s$–$z$ transition sets in before the $\Pi_1(\rho)$ loop has been completed. The interpretation of this result is that the $g$–$l$ and the $s$–$z$ transitions have merged into one ("$g$–$z$") transition from the gas to the condensed liquid phase. This rather common case is characterized by a large jump in $\Delta$, typically from $\Delta_g \sim 0$ to (nearly) the maximal value, $\Delta_z \cong 1 - P_z^0$. The corresponding jump in $\rho$ is also large. A very similar behavior prevails in systems where $T_c^{g-l} < T_c^{s-z}$ and $\rho_c^{s-z}$ is small ($\rho_c^{s-z} \gtrsim \rho_c^{g-l}$). In this case the $g$–$l$ coexistence curve is nearly fully absorbed into the $s$–$z$ curve, so that the $s$–$z$ transition preempts the $g$–$l$ transition at all $T < T_c^{s-z}$. (In this case the distinction between an $s$–$z$ or $g$–$z$ transition is meaningless). An example

of this behavior was shown in Fig. 5. The opposite case, where only a $g$–$l$ transition can take place is, of course, also possible. As an extreme example we may take a system where the interaction parameters (in our model) $w_{zz}$, $w_{ss}$, and $w_{zs}$ are all negative but $w_{zz} + w_{ss} - 2w_{zs} = W = 0$. Then, of course, the monolayer can only undergo a $g$–$l$ transition, since the $s$–$z$ transition is impossible [$W \to 0$ implies $T_c^{s-z} \to 0$ or $\rho_c^{s-z} \to \infty$, cf. Eqs. (47) and (48)]. Thus in systems with small $W$ one expects that at densities $\rho > \rho_l$ the order parameter $\Delta$ will increase monotonically with $\rho$. This behavior has indeed been revealed by our Monte Carlo simulations, see, e.g., Fig. 1.

We close the mean-field analysis with some comments on the role of the molecular parameters, particularly $\epsilon$ and $\alpha$, in the monolayer's phase behavior. The qualitative conclusions drawn here pertain also to the Monte Carlo simulations presented in the next section.

Consider first the limit of large adsorption energy, say $(\chi - 1)\epsilon = \ln(P_s^0/2P_z^0) \gtrsim 1$. In this case the rods stick to the surface and are reluctant to stand up. They are forced to do so, however, by the strong excluded area repulsions when $\rho \to \tilde{\rho} \simeq 1/\langle b \rangle$. Since in this case $\langle b \rangle$ is large, $\langle b \rangle \cong b_{ss} = (b_{xx} + b_{xy})/2 = (\chi^2 + 6\chi + 1)/4$, [see Eq. (22)], the corresponding density $\tilde{\rho} = 1/b_{ss}$ is small; e.g., for $\chi = 4$ we get $\tilde{\rho} \simeq 0.1$. For the fraction of occupied area at this point we find $\tilde{\phi} \simeq \chi\tilde{\rho} \simeq \chi/b_{ss}$. If rod–rod attractions in the $xy$ plane are strong enough ($T < T_c^{g-l}$) the monolayer can complete a $g$–$l$ transition (with all rods in the plane) before the density reaches $\tilde{\rho}$, i.e., with $\rho_g < \rho_l < \tilde{\rho}$. Estimates of $T_c^{g-l}$ and $\rho_c^{g-l}$ for the case of large $\epsilon$ can be obtained from Eq. (17) with $\langle b \rangle$ and $\langle a \rangle$ replaced by the constant coefficients $b_{ss}$ and $a_{ss}$; namely $kT_c^{g-l} = 8a_{ss}/27b_{ss}$ and $\rho_c^{g-l} = 1/3b_{ss}$, both familiar from the usual vdW theory. The numerical values obtained, e.g., for $\chi = 4$ are $kT_c^{g-l} = 1/u_c^{g-l} \cong 0.36$ and $\rho_c^{g-l} \simeq 0.032$.

Large $\epsilon$ tends to postpone the $s$–$z$ transition to higher densities, due to the reluctance of the rods to give up their adsorption energy. This is reflected by the increase of $\phi_c^{s-z}$ with $\epsilon$, as shown in Fig. 4. As we have seen in the previous section, excluded area interactions in the monolayer (unlike in 3D) do not provide a sufficient incentive for a first-order orientational transition. A necessary condition for such a transition is a strong anisotropic attractive potential $W$. If $W$ is such that the coexisting phases in the $s$–$z$ transition satisfy $\rho_l < \rho_1 < \rho_c^{s-z} < \rho_2 < 1$ then, indeed, a first-order $s$–$z$ transition will follow the $g$–$l$ transition. This sequence of inequalities is satisfied over a limited range of molecular parameters. For $\chi = 4$ and, say, $\epsilon = 4/3$ and $u = 3$, this condition is fulfilled for $\alpha \simeq 2$, as we have already seen in Fig. 7. However, if $\alpha$ and therefore also $W$ are smaller, say $\alpha \simeq 1$, one finds that $\rho_1 > 1$, which means that a first-order $s$–$z$ transition occurs only at physically unacceptable densities. (This trend is also reflected by the sharp increase in $\phi_c$ as $\alpha$ changes from 2 to 1, Fig. 4.) We thus conclude that in this case, following the $g$–$l$ transition, $\Delta$ increases *continuously* with $\rho$. On the other hand, if the anisotropic attraction is very large, say $\alpha = 4$, then for the same values of $\chi$, $\epsilon$, and $u$ as above, the onset of the $s$–$z$ transition shifts to very low densities, resulting in $\rho_1 < \rho_l$ or even $\rho_c^{s-z} < \rho_l$. This is a case of a system showing a single ($g$–$z$) first-order transition.

As $\epsilon$ decreases the fraction, $P_s^0 + \Delta$, of surface rods in the plane decreases and likewise their resistance to stand up as $\rho$ increases. This results in increasing values of $\rho_c^{g-l} \simeq 1/3b(\rho_c)$ and $\rho_l \simeq 1/b(\rho_l)$. In parallel, when $\epsilon$ decreases the $s$–$z$ transition is shifted to lower densities, i.e., $\rho_c^{s-z}$ (and $\rho_1$) decrease, as shown in Fig. 4. As a consequence of this overlap between the (coexistence curves of the) $g$–$l$ and $s$–$z$ transitions they merge into one, $g$–$z$, transition.

To summarize, our analysis suggests that large $\epsilon$ is a necessary condition for the appearance of two, successive, first order transitions. In addition, however, the strength of the anisotropic attraction (as measured by $W$, or $u$ and $\alpha$) which determines the shape of the $s$–$z$ coexistence curve should not be too small (in which case it is largely absorbed into the the $g$–$l$ coexistence curve) nor too large (in which case the $s$–$z$ absorbs the $g$–$l$ transition).

## IV. MONTE CARLO SIMULATIONS

In this section we present the results of Monte Carlo simulations for some representative systems of mobile grafted rods. The computations are performed on the same restricted-orientation lattice model which we have used since Sec. II. The motivation for carrying out full MC simulations on the *restricted* orientational model is that we want to confirm as directly as possible the mean-field conclusions, involving the possibility for successive fluid–fluid phase transitions.

Recall that the $xy$ plane (the surface) is represented by a square lattice, each site of which (of area $d^2 = 1$) can accommodate one rod in the upright ($z$) orientation. When adsorbed on the surface a rod occupies $\chi$ consecutive sites parallel to the $x$ or the $y$ axes. The adsorption energy per "segment" in contact with the surface is $\epsilon kT$, e.g., $\chi\epsilon kT$ for a lying-down rod and $\epsilon kT$ for a standing-up one. The restriction of one rod segment per lattice site implies the *same* excluded area interactions specified in Eq. (22). Similarly, by treating the attraction between rods as a sum of nearest-neighbor segment–segment potentials we obtain complete correspondence with Eq. (24). More explicitly, for the attractive potential between a pair of rods in a given configuration we take $u_a = -nukT$, where $n$ is the number of nearest-neighbor segment–segment contacts, see Eq. (4). The only exception is the configuration of two rods in the $z$ state for which case instead of $u$ we take $\alpha u$, $\alpha > 1$. If we substitute this $u_a$ into Eq. (8) we obtain Eq. (24). [Note, however, that other choices of $u$ could also lead to Eq. (24)].

Although the interaction potentials in the lattice simulations and the mean-field analysis are entirely equivalent, we clearly do not expect more than a qualitative agreement between the two approaches. It should be recalled that following the basic approximation of using Eq. (9) for $F$ we have made two additional approximations. First, we employed an approximate scheme to separate (in Sec. III A) and then to combine (in Sec. III C) the gas–liquid and the standing-up transitions. Second, in order to eliminate from the discussion the complexities associated with rod alignment and phase transitions in the $xy$ plane, we have consistently assumed $P_x = P_y$ (hence $F_{xy} \equiv 0$). This assumption

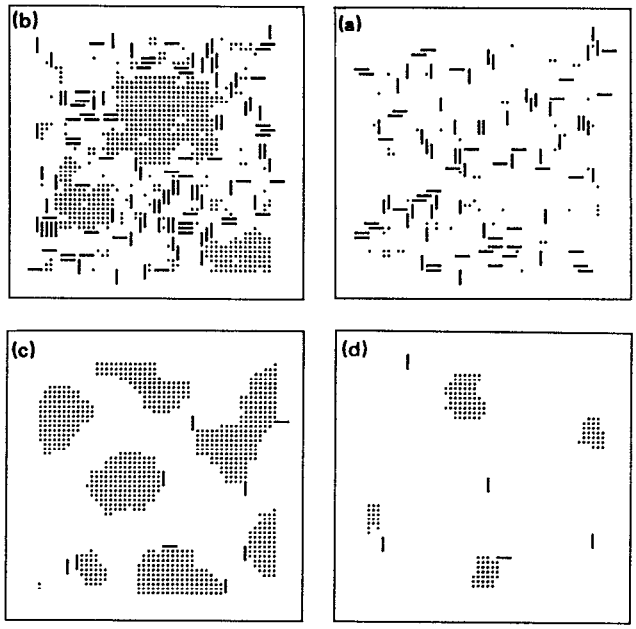


FIG. 8. Snapshots of typical configurations from a Monte Carlo simulation of rod monolayers with $\chi = 4$, $\epsilon = 0$, and $\alpha = 1$. (Shown are $50 \times 50$ sections from the simulation of a $100 \times 100$ lattice.) Figures (a)–(d) correspond to the four thermodynamic states ($a,b,c,d$) in the temperature ($1/u$) vs area ($\sim 1/\rho$) phase diagram of Fig. 9(a). Specifically, points (a)–(d) correspond, respectively, to $(u,\rho) = (0.5,0.05)$, $(0.5,0.3)$, $(1.0,0.3)$, and $(1.0,0.05)$. Note that point (a) describes a homogeneous phase whereas (b)–(d) are in the two-phase region.

can be rigorously incorporated into the simulations if the surface particles are chosen to be symmetrical e.g., squares. We shall do so after first discussing the case of rods which are free to lie in the plane along $x$ or $y$ or stand up along $z$. The rods are indeed found to order in the plane at high densities, forming in some cases tilelike patterns, which are explained below. Such patterns cannot be explained by a simple mean-field approach, even one which allows $P_x \neq P_y$.

All the simulations reported here were carried out according to the standard (Metropolis) procedure.[31] The lattice size used was $100 \times 100$ in all cases, except where larger samples ($200 \times 200$) were used to verify that finite size effects are unimportant. The simulations are performed in the $N,V,T$ ensemble. When results for chemical potentials are reported they were calculated using Widom's insertion method.[32] For all the systems and all the initial conditions studied, the typical duration of a simulation run was $\sim 10^6$ Monte Carlo steps (MCS), with each step corresponding to a sweep through all the particles. In each MCS every particle is allowed (on the average) one attempted move, corresponding to either a change of orientation, or translation by one lattice site on the surface. The simulations were performed on Silicon Graphics workstations.

The results of the simulations for a monolayer of hard ($u \neq 0$) rods were shown already in Figs. 1 and 2. These simulations confirm the prediction of the mean-field analysis that an orientational phase transition does not take place in this system. Clearly, a $g$–$l$ transition does not take place either since there is no attraction between rods, in the several cases involved there.

Figure 8 shows four snapshots from a simulation of a monolayer with $\chi = 4$, $\epsilon = 0$, and $\alpha = 1$. This is a typical case of a system with low adsorption energy, for which, based on the discussion in the previous section, we expect a single ("$g$–$z$") first-order phase transition. The figures clearly illustrate the phase separation process attendant upon cooling or compressing the system into the coexistence region. In discussing them it is useful to refer to the temperature ($\sim 1/u$) vs area ($\sim 1/\rho$) phase diagram shown in Fig. 9(a). In particular, Figs. 8(a)–8(d) display typical configurations for the thermodynamic states indicated by points a–d in Fig. 9(a). Note that Fig. 8(a) involves a uniform density gas phase in which standing-up and lying-down rods are mixed throughout the available area. Indeed, point $a$ corresponds to the one phase, high-temperature and large-volume (gas) region in the $T$–$\rho$ diagram shown in Fig. 9(a).

Upon either compressing (at constant temperature) to point $b$ in Fig. 9(a), or cooling (at constant density) to point $d$, the system is brought into the two phase region involving coexistence between the gas phase discussed for Fig. 8(a) and a highly condensed phase in which essentially all the rods are standing-up—see Figs. 8(b) and 8(d). Moving

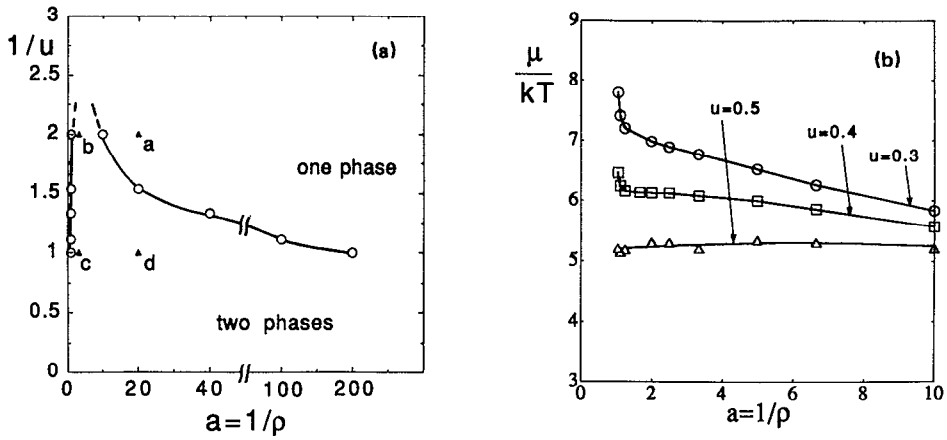


FIG. 9. (a) Temperature ($1/u$) vs area ($1/\rho$) phase diagram obtained by Monte Carlo simulations (see the text) for the monolayer ($\chi = 4$, $\alpha = 1$, $\epsilon = 0$) of Fig. 8. (b) Three chemical potential isotherms for the above system corresponding to monolayers above ($u = 0.3$) below ($u = 0.5$) and, approximately, at the critical temperature ($u = 0.4 \sim u_c$).

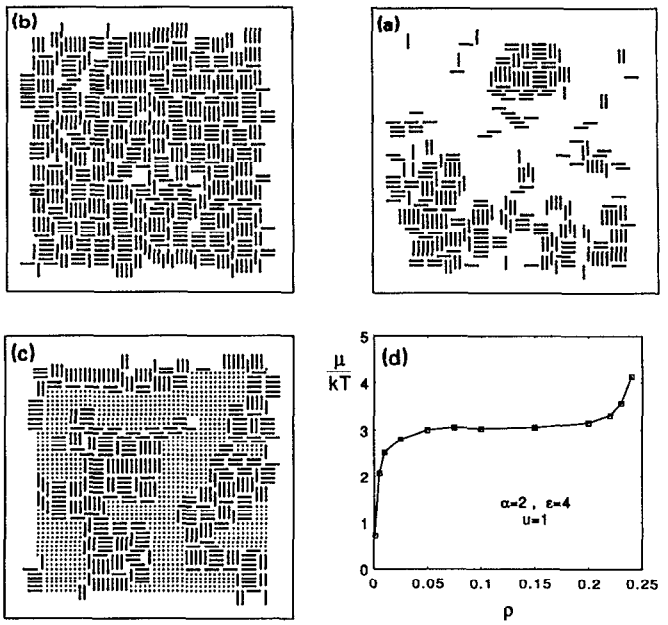


FIG. 10. Typical configurations (50×50 sections from 100×100 samples of Monte Carlo simulations) of a monolayer exhibiting two first order transitions. The three figures correspond to isothermal compressions of a rod monolayer with $\chi = 4$, $\alpha = 2$, $\epsilon = 4$, $u = 1$. (a) Coexistence between a gas phase and (islands of) expanded-liquid phase of lying-down rods. (b) The monolayer pattern at the end of the above, *g–l*, transition and, just before the next, *s–z*, transition sets in. (c) Coexistence between a *z* (liquid-condensed) phase, of standing-up rods and an *s* (liquid-expanded) phase consisting of lying-down rods. (d) The chemical potential in the gas–liquid transition region.

horizontally from point *d* to *c* describes an isothermal compression which simply involves the "growth" of the condensed phase according to the usual lever rule. The differences in density $\rho_z - \rho_g$ and order parameter $\Delta_z - \Delta_g$ decrease as $T$ ($\sim 1/u$) approaches the critical point. The coexistence curve ($T$–$\rho$ diagram) in Fig. 9(a) was determined by analysis of computer experiments corresponding to isothermal compression and isochoric cooling. The analysis comprised inspection of snapshots of the kind shown in Figs. 8(a)–8(d), as well as the calculations of $\mu = \mu(T,\rho)$, collected in Fig. 9(b). For each $T,\rho$ point shown, $\mu$ was evaluated by averaging the results of $\sim 10^6$ insertion attempts over several (typically ten) different configurations of the monolayer. The accuracy of the calculations decreases around the critical point.

Figure 10 confirms the qualitative notion that large adsorption energy is a necessary requirement for the appearance of *two*, successive, transitions. The snapshots (a)–(c) shown correspond to isothermal compression (at $u = 1$) of a monolayer characterized by $\chi = 4$, $\alpha = 2$, and $\epsilon = 4$. Various other choices of monolayer parameters (e.g., $\alpha,\epsilon,u = 1,1,1.25$, or $\alpha,\epsilon,u = 2,3,0.85$ for $\chi = 4$) reveal similar qualitative behavior. Namely, a *g–l* transition sets in at low densities, with negligible change in the orientational order parameters, $\Delta_g \cong \Delta_l \cong 0$. Figure 10(a), with $\rho = 0.1$, lies already in the two phase gas–liquid region, revealing coexistence between low- and high-density fluids of lying down ($\Delta \cong 0$) rods. Figure 10(d) shows the chemical potential of the system in the density regime corresponding to the gas–liquid phase transition. The flat portion of $\mu$ confirms the coexistence of the two phases. Note that $\rho_l \lesssim 1/\chi$ in the liquid domains, corresponding to a situation where essentially all of the area in the domains is covered by lying down rods. Equivalently, the coverage $\phi$, cf. Eq. (42), is nearly completely saturated: $\phi_l \cong \chi\rho_l \lesssim 1$.

Consequently, we expect that the *orientational* transition, involving a standing up of the lying-down rods, will set in shortly after the condensation from the gas to liquid is complete, i.e., when the system density begins to exceed $\rho_l \cong 1/\chi$ ($= 0.25$ in our present example). Figure 10(b) shows a typical configuration just before reaching this point: $\rho = 0.24 \lesssim \rho_l$. For higher densities (and still at the same temperature, i.e., same $u$ and $\epsilon$) we move into the two phase region involving coexistence with essentially full-coverage standing-up rods ($\rho_2 \lesssim 1$ and $\Delta_2 \lesssim 1$). Figure 10(c) shows a typical configuration in this two phase region, at an overall system density of $\rho \cong 0.54$ corresponding, roughly, to comparable amounts of the two phases. Simulations performed at lower temperatures, (large $u$) reveal (e.g., when $u = 2, \epsilon = 3$, and $\alpha = 2$) that instead of two successive transitions the monolayer exhibits only a single jump from gas to condensed liquid. This corresponds to $T < T_{tp}$ as discussed at the end of Sec. III C.

The numerical value of the liquid phase density, $\rho_l \sim 1/\chi$, found in the simulations is considerably larger than the mean-field estimate $\rho_l \sim 1/b_{ss}$. One of the many reasons for this difference is our assumption, $P_x = P_y$, that rod orientations in the plane are random [or, $\eta = 0$, cf. Eq. (34)]. This assumption eliminated the possibility in the mean-field theory of long range in-plane order which would imply smaller $b_{ss}$, i.e., $b_{ss} \sim b_{xx}$ instead of $b_{ss} \equiv (b_{xx} - b_{xy})/2$. Relaxing this assumption cannot dramatically improve the agreement between the mean-field and simulation results, because of the rather special (in-plane) rod–rod correlations apparent from the monolayer patterns of the "liquid-expanded" ("*s*") phase, see Figs. 10(a)–10(c).

Figure 10 reveals in-plane ordered domains of the liquid-expanded ($\rho \cong 1/\chi$) phase, consisting, roughly, of $\chi$ by $\chi$ "tiles" of parallel rods. To a large extent this is an artifact of our restricted-orientation lattice model which does not allow for (small) fluctuations in rod orientations.[33] Each of those clusters of $\chi$ parallel rods is essentially randomly oriented with respect to the others since their alignment involves no further advantage as far as the excluded area interactions are concerned. Similarly, since in our model the attractive interactions are sums of nearest-neighbor segment–segment potentials, the total potential energy is *also* unaffected by long-range ordering of these tiles at this density. Consequently, there is no driving force for *long-range* nematic order in the restricted orientation model. Yet, the "tiling" phenomenon complicates the mean-field analysis. It does not change, however, our conclusion that the first discontinuous transition which occurs is an in-plane condensation of particles while the second involves their standing up off the surface. To demonstrate this point clearly it is instructive to treat a system where this artifact cannot arise, e.g., the "che-

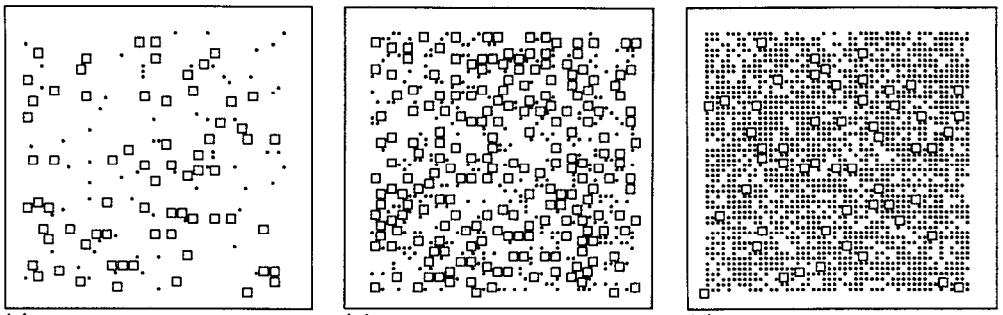


FIG. 11. Three typical configurations from a Monte Carlo simulation of a mixture of interconverting *hard* squares. ($\chi = 4$, $u = 0$, and $\epsilon = 0$, corresponding to $P_s^0/P_z^0 = 2$). Shown are $50 \times 50$ sections from the $100 \times 100$ lattices used in the simulations. Note the *continuous* increase in the fraction of small rods $P_z = 1 - P_s$, as the density increases from $\rho = 0.05$ in (a), to 0.2 in (b) to 0.7 in (c).

mically reactive" mixture of squares mentioned earlier.

More explicitly, we continue to treat the upright ($z$) rods as particles occupying a single lattice site in the $xy$ surface, or more specifically, as elongated parallelepipeds of length $\chi = l$ and square cross section $d \times d = 1$. We replace the $x$ and $y$ rods by flat parallelepipeds ($s$ particles) of area $\chi = \sqrt{l} \times \sqrt{l}$ and height $d = 1$. Thus the volume of the $z$ and $s$ particles is the same, as if they were chemical isomers of some molecule. The projection of the particles on the $xy$ plane corresponds to a mixture of interconverting small and large squares.

We keep assuming that the repulsive interactions are of the excluded-area type: zero if the squares do not overlap and infinite otherwise. Similarly the adsorption energy per segment is $\epsilon$, i.e., $l^2\epsilon$ and $\epsilon$ for a big and a small square, respectively. As in Eq. (21) we assume that the $s$ state is doubly degenerated so that $P_s^0 = 2P_z^0$ when $\epsilon = 0$. Clearly, this is an arbitrary choice made only for comparative purposes. Finally, the attractions between particles are again a sum of nearest-neighbor contributions, with $-ukT$ from each such segment–segment pair. Thus the attraction energy between two adjacent small squares is $-\chi ukt$ (we consider only $\alpha = 1$ in this model) or $-ukT$ between neighboring large and small squares, etc.

We have already remarked in our generalized van der Waals discussion for reorienting rods [see the paragraph before Eq. (36)] that the quasianalytical development presented there can be carried over directly to this system of bidisperse, "chemical reacting," squares. The **a** and **b** matrices are easily evaluated and consequent results can be derived for the attending phase behavior. Here, however, we shall illustrate the relevant analogies by simply presenting the data generated by MC simulations of this system. The simulations are completely analogous to those of the rod system. In each MC move an attempt is made to either translate a particle or to change its size (from big to small or vice versa), with acceptance probability according to the Metropolis criterion.

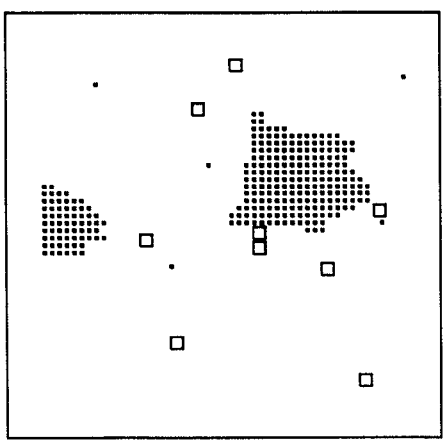

FIG. 12. A typical configuration from a Monte Carlo simulation of a mixed monolayer of attracting, interconverting small and large squares. This monolayer ($\chi = 4$, $\epsilon = 0$, and $u = 1$) exhibits one first order phase transition.

At low number densities, where the average distance between squares is much greater than their sizes, one expects that most of the particles will be large ones since interparticle interactions are not important and it is essentially the single-particle, adsorption energy, which must be minimized. On the other hand, as the density approaches the close packing value for small squares, (i.e., $\rho \to 1$), the small squares become the dominant species because of excluded area packing constraints. It remains "only" to determine whether this progression occurs continuously or via one first-order or two successive first-order phase transitions.

Figures 11(a)–11(c) show three typical Monte Carlo configurations for low, intermediate and high densities, i.e., $\rho = 0.06$, 0.2, and 0.7, in the case of pure excluded area interactions ($u = 0$ and $\epsilon = 0$). The two square sizes are $2 \times 2$ and $1 \times 1$. It is clear that the progression from large to small squares is continuous and that no phase transition occurs. Allowing for $\epsilon > 0$ has no effect other than to make the small squares less likely at low density, just as in the one-component rod case it resulted only in a larger fraction of lying-down rods in the dilute regime. In the absence of interparticle attractions ($u = 0$) we again find that the standing up of particles ($s \to z$ rods or large $\to$ small squares) occurs continuously.

As soon as attractions are introduced ($u \neq 0$), the possibility arises for a first-order phase transition. Figure 12 shows a typical configuration of coexistence phases of $2 \times 2$ and $1 \times 1$ squares at $\rho = 0.05$ for $u = 1.0$ and $\epsilon = 0$. The behavior of this system is analogous to the one described in Fig. 8 where the compression (or cooling) of one-component rods with $u \neq 0$ and $\epsilon = 0$ involved a single phase transition to a standing-up state.

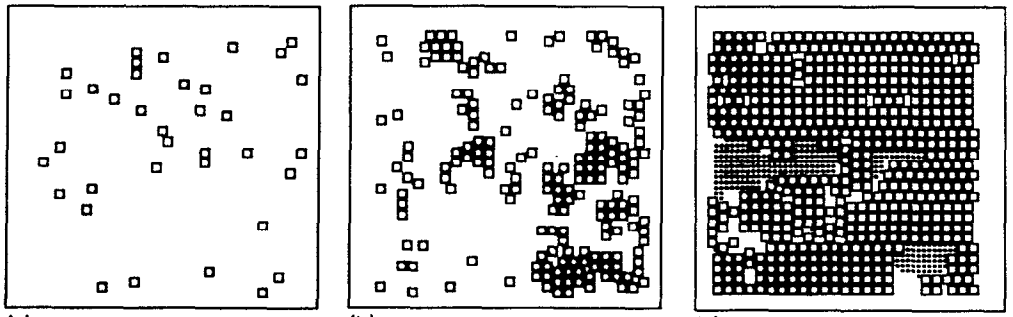


FIG. 13. Typical configurations from a Monte Carlo simulation of a mixed monolayer of interconverting squares which exhibit two successive transitions. The monolayer parameters are $\chi = 4$, $\epsilon = 4/3$, and $u = 1$. (a) $\rho = 0.01$; gas phase of large (strongly adsorbing) squares. (b) $\rho = 0.1$; coexistence between gas and (islands of) an expanded liquid phase. (c) $\rho = 0.3$; coexistence between expanded and condensed (small squares) liquid phases.

Finally, with the addition of a sufficiently strong adsorption energy ($\epsilon \neq 0$) the progression from big to small squares is characterized by *two*, successive, first-order phase transitions. Figures 13(a)–13(c) show this sequence for the case of $u = 1.0$ and $\epsilon = 4/3$. Note that we move upon compression from a gas phase of big squares at $\rho = 0.01$ [see Fig. 13(a)] to a two-phase coexistence at $\rho = 0.1$ involving dilute and condensed phases of big squares (b), and then finally to a two-phase coexistence consisting of two condensed phases of big and small squares, respectively [Fig. 13(c)] This behavior is the analog of that shown in Figs. 10(a)–10(c) and discussed there in terms of a gas-liquid condensation (of lying-down rods) followed by a transition to standing-up rods. Further details about the phase behavior of a system of interconvertible symmetric particles will be published elsewhere.[34]

## ACKNOWLEDGMENTS

We would like to thank Julian Talbot and Zhen-Gang Wang for many helpful discussions during the early stages of this work. We thank the Israel–United States Binational Science Foundation (Grant Number 87-17113), and the National Science Foundation (Grant Number CHE-88-16059) for financial support. The Fritz Haber Center is supported by the Minerva Gesellschaft für die Forschung, Munich Germany.

## APPENDIX: THE GENERALIZED VAN DER WAALS EQUATION

In this section we briefly outline the approximations and assumptions involved in the derivation of the generalized van der Waals and virial equations for the free energy and pressure of a monolayer of mobile grafted rods. Although most of the relevant concepts and notions are well known, we find it instructive to present them in a form appropriate for the model calculations and computer simulations presented in the present paper.

The number of indistinguishable configurations $\mathbf{r}^N$, $\Omega^N$ corresponding to the same orientational distribution (composition) $\{N_\Omega\}$ is $\Pi N_\Omega!$. Thus the classical configurational partition function of a monolayer of a given composition $\{N_\Omega\}$ is

$$Z(\{N_\Omega\},A,T) = \frac{1}{\Pi N_\Omega!}\int d\mathbf{r}^N \exp[-\beta U(\mathbf{r}^N,\Omega^N)], \tag{A1}$$

where $U$ is the total potential energy of the rod mixture, cf. Eq. (1), $\beta = 1/kT$, and $A$ is the total area available to the $N$ molecules of the system. The total configurational integral is the sum over all compositions $Z(N,A,T) = \Sigma Z(\{N_\Omega\},A,T)$. In the thermodynamic limit $\ln Z(N,A,T) \to \ln Z(\{N^*_\Omega\},A,T)$, with $Z(\{N^*_\Omega,A,T)$ denoting the maximal term in the sum. $\{N^*_\Omega\}$ is the most probable, i.e., the equilibrium, composition. Hence the system free energy is

$$F = -kT \ln Z(\{N^*_\Omega\},A,T). \tag{A2}$$

The equilibrium composition is determined by minimizing $F$ with respect to the appropriate order parameters.

Substituting $U$ from Eq. (1) into Eq. (A-1) and noting that $\Sigma_i \epsilon(\Omega_i) = \Sigma_\Omega N_\Omega \epsilon(\Omega)$ we can write

$$Z = Z_{\rm hr} Z_a^{\rm (hr)} \tag{A3}$$

with

$$Z_{\rm hr}(\{N_\Omega\},A,T) = \prod_\Omega \left[\frac{e^{-\beta N_\Omega \epsilon(\Omega)}}{N_\Omega!}\right]\int d\mathbf{r}^N \times \exp\left[-\beta \sum_{i<j} u_r(\mathbf{r}_{ij},\Omega_i,\Omega_j)\right] \tag{A4}$$

denoting the configurational partition function of a monolayer of hard rods. The product in front of the integral is simply the partition function of a monolayer of noninteracting rods.

The second factor in Eq. (A3) includes the contributions of the attractive potentials, averaged in the hard rod system. That is,

$$Z_a^{\rm (hr)} = \int d\mathbf{r}^N P_{\rm hr}(\mathbf{r}^n,\Omega^n)\exp\left[-\beta \sum_{ij} u_a(\mathbf{r}_{ij},\Omega_i,\Omega_j)\right], \tag{A5}$$

where $P_{\rm hr}(\mathbf{r}^N,\Omega^N) \sim \exp[-\beta \Sigma_{i<j} u_r(\mathbf{r}_{ij},\Omega_i,\Omega_j)]$ is the $N$-body probability in the hard-rod system.

Expanding the exponents in Eq. (A5) in powers of $\beta u_a$ and neglecting $0(\beta^2)$ terms we find that the contribution of the attractive potential to the free energy is given by

$$F_a^{(\mathrm{hr})} = -kT \ln Z_a^{(\mathrm{hr})} \cong \sum_{i<j} \langle u_a(\mathbf{r}_{ij},\Omega_i,\Omega_j)\rangle_{\mathrm{hr}}$$

$$= \tfrac{1}{2}N\rho \sum_{\Omega} \sum_{\Omega'} P_\Omega P_{\Omega'} \int d\mathbf{r}\, g_{\mathrm{hr}}(\mathbf{r},\Omega,\Omega') u_a(\mathbf{r},\Omega,\Omega')$$

$$= N \sum_{\Omega} P_\Omega \Psi(\Omega). \tag{A6}$$

In the last equation, $\langle\ \rangle_{\mathrm{hr}}$ indicates averaging according to the probability distribution $P_{\mathrm{hr}}(\mathbf{r}^n,\Omega^N)\cdot g_{\mathrm{hr}}(\mathbf{r},\Omega,\Omega')$ is the radial distribution function for a pair of rods in orientations $\Omega$ and $\Omega'$. The last equality serves as the definition of the effective (mean-field) attractive potential felt by a rod in orientation $\Omega$, cf. Eq. (5).

The next approximation is to replace $g_{\mathrm{hr}}$ by its low density limit

$$g^0(\mathbf{r}_{ij},\Omega_i,\Omega_j) = \exp[-\beta u_r(\mathbf{r}_{ij},\Omega_i,\Omega_j)]$$
$$= 1 + f_{\mathrm{hr}}(\mathbf{r}_{ij},\Omega_i,\Omega_j), \tag{A7}$$

which implies $g^0 = 0$ or 1 for overlapping and non overlapping rod configurations, respectively. $f_{\mathrm{hr}}(i,j)$ is the Mayer function for a pair of hard rods. From Eqs. (A6) and (A7) one gets

$$\beta F_a^{(\mathrm{hr})}/N = -\beta \langle a\rangle \rho \tag{A8}$$

with the orientationally averaged $a$ coefficient defined in Eq. (8) of Sec. II.

Finally, to derive the generalized vdW equation the integral in Eq. (A4) is replaced by the mean-field product, yielding

$$Z_{\mathrm{hr}} = \prod_{\Omega} \left[\frac{e^{-\beta N_\Omega \epsilon(\Omega)}}{N_\Omega!}\right] [A - N\langle b\rangle]^N \tag{A9}$$

with $\langle b\rangle$ denoting the average vdW $b$ coefficient defined in Eq. (7) of Sec. II. Equation (6) then follows from $F = -kT \ln Z$ using Eqs. (A3), (A8), and (A9).


[1] G. L. Gaines, *Insoluble Monolayers at Liquid Gas Interface* (Wiley, New York, 1966).
[2] For a recent review, see, C. Knobler, Adv. Chem. Phys. 77, 397 (1990).
[3] (a) See, for example, N. R. Pallas and B. A. Pethica, J. Chem. Soc. Faraday Trans. 1 **83**, 585 (1987); (b) N. R. Pallas and B. A. Pethica, Langmuir **1**, 509 (1985).
[4] B. C. Moore, C. M. Knobler, S. Akamatsu, and F. Rondelez, J. Phys. Chem. **94**, 4588 (1990).
[5] K. Kjaer, J. Als-Nielsen, C. A. Helm, L. A. Laxhuber, and H. Möhwald, Phys. Rev. Lett. **58**, 2224 (1987).
[6] For the phase behavior in the high density regime see, for example, (a) H. M. McConnell and V. T. Moy, J. Phys. Chem. **92**, 4520 (1988); (b) A. Fischer and E. Sackmann, J. Phys. (Paris) **45**, 517 (1984); (c) J. P. Bareman, G. Cardini, and M. L. Klein, Phys. Rev. Lett. **60**, 2152 (1988); (d) K. Kjaer, J. Als-Nielsen, C. A. Helm, P. Tippman-Krayer, and H. Möhwald, J. Phys. Chem. **93**, 3200 (1989).
[7] J. Daillant, L. Bosio, B. Harzallah, and J. J. Benattar, J. Phys. II, **1**, 149 (1991).
[8] I. Szleifer, A. Ben-Shaul, and W. M. Gelbart, J. Phys. Chem. **94**, 5081 (1990).
[9] S. Shin, Zhen-Gang Wang, and S. A. Rice, J. Chem. Phys. **92**, 1427 (1990).
[10] (a) R. S. Cantor and P. M. McIlroy, J. Chem. Phys. **90**, 4423 (1989); (b) **90**, 4431; (c) **91**, 416 (1989).
[11] C. M. Roland, M. J. Zuckermann, and A. Georgallas, J. Chem. Phys. **86**, 5812 (1987).
[12] D. P. Fraser, O. G. Mouritsen, and M. J. Zuckermann, Phys. Scr. T **33**, 81 (1990).
[13] See, for example, G. M. Bell, L. L. Combs, and L. J. Dunne, Chem. Rev. **81**, 15 (1981).
[14] A. Caille, D. Pink, F. DE Verteuil, and M. J. Zuckermann, Can. J. Phys. **58**, 581 (1980).
[15] M. E. Costas, Z. G. Wang, and W. M. Gelbart, J. Chem. Phys. **96**, 2228 (1992).
[16] R. E. Boehm and D. E. Martire, J. Chem. Phys. **67**, 1061 (1977).
[17] (a) A. Halperin, I. Schechter, and S. Alexander, J. Chem. Phys. **86**, 6550 (1987); **91**, 1383 (1989); see also, B. C. Moore, *ibid.* **91**, 1381 (1989).
[18] Z-Y. Chen, J. Talbot, W. M. Gelbart, and A. Ben-Shaul, Phys. Rev. Lett. **61**, 1376 (1988).
[19] Z-G. Wang, J. Phys. (Paris) **51**, 1431 (1990).
[20] R. L. Coldwell, T. P. Henry, and C. W. Woo, Phys. Rev. A **10**, 897 (1974).
[21] L. Onsager, Ann. N. Y. Acad. Sci. **51**, 625 (1949).
[22] R. W. Zwanzig, J. Chem. Phys. **39**, 1714 (1963).
[23] (a) D. Frenkel and R. Eppenga, Phys. Rev. A **31**, 1776 (1985); (b) A. Stroobants, H. M. W. Lekkerkerker, and D. Frenkel, *ibid.* **36**, 2929 (1987); (c) J. A. Cuesta and D. Frenkel, *ibid.* **42**, 2126 (1990).
[24] E. A. DiMarzio J. Chem. Phys. **35**, 658 (1961).
[25] (a) W. M. Gelbart and B. A. Baron, J. Chem. Phys. **66**, 207 (1977); (b) M. A. Cotter, *ibid.* **66**, 4710 (1977).
[26] M. Kac, G. E. Uhlenbeck, and P. C. Hemmer, J. Math. Phys. **4**, 216 (1963).
[27] H. C. Longuet-Higgins and B. Widom, Mol. Phys. **8**, 549 (1964).
[28] W. Maier and A. Saupe, Z. Naturforsch. Teil A **14**, 882 (1959).
[29] S. K. Ma, *Statistical Mechanics* (World Scientific, Singapore, 1985).
[30] T. L. Hill, *Statistical Mechanics* (McGraw-Hill, New York, 1956).
[31] N. Metropolis, A. W. Rosenbluth, M. N. Rosenbluth, A. N. Teller, and E. Teller, J. Chem. Phys. **21**, 1087 (1953).
[32] B. Widom, J. Chem. Phys. **39**, 2808 (1963).
[33] See, for example, Fig. 2.6 and attendant discussion of the restricted-orientation lattice model of the 3D isotropic→nematic transition in P. G. de Gennes, *The Physics of Liquid Crystals* (Clarendon, Oxford, 1974).
[34] D. Kramer, A. Ben-Shaul, and W. M. Gelbart (to be published).